

TRANSIENT FLOW ANALYSIS  
OF REACTION CONTROL SYSTEM  
FOR APOLLO LUNAR MODULE

CONTRACT NAS9-6666

FOR

NATIONAL AERONAUTICS AND SPACE ADMINISTRATION

Auxiliary Propulsion and Pyrotechnics Branch

Propulsion and Power Division

MANNED SPACECRAFT CENTER

HOUSTON, TEXAS

BY

LAMAR STATE COLLEGE OF TECHNOLOGY

RESEARCH CENTER

BEAUMONT, TEXAS

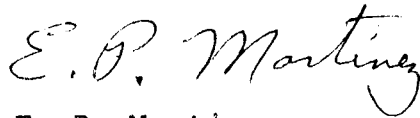
JULY, 1968



## FOREWORD

This report documents work done for NASA-MSC, Houston, Texas, under contract NAS9-6666 with the Research Center of Lamar State College of Technology. The realization of contract objectives was initially dependent upon programming and computing services of the Hybrid Techniques Section, Computation and Analysis, MSC. Unsuccessful hybrid computing attempts necessitated several time extensions of the contract and greater emphasis on computing techniques by the contractor. A digital computer program prepared by Dr. Fred M. Young at Lamar Tech enabled numerical results to be obtained. Hence, the original objectives of developing a simulation capability for the L/M-RCS system and utilizing the simulation on a computer were all accomplished at Lamar Tech.

Activities were coordinated by Mr. Chester A. Vaughan, Head, Reaction Control Systems Section, Propulsion and Power Division, MSC. He was assisted by Mr. Lonnie W. Jenkins of the same group.



E. P. Martinez  
Principal Investigator  
Lamar State College of Technology

## ABSTRACT

A lumped parameter description of the propellant feed system for the L/M-RCS is presented. A simple two-phase model for transient flow analysis of an injector is developed. The injector model couples the feed line description to an existing engine combustor model, providing a system simulation capability.

The results of a digital computer simulation are presented for several combinations of system parameters. Qualitative and quantitative agreement with experimental results is within expectations for the scope of the models.

Recommendations are made for improving the quantitative capability of the simulation models.

# TABLE OF CONTENTS

<u>Topic</u>	<u>Page</u>
Foreword . . . . .	i
Abstract . . . . .	ii
Table of Contents . . . . .	iii
Introduction . . . . .	1
Method of Analysis . . . . .	9
Feed System . . . . .	9
Injectors . . . . .	16
Combustor . . . . .	23
Reaction Control System . . . . .	24
Results . . . . .	28
Hybrid . . . . .	28
Digital . . . . .	28
Runs 1 and 15 . . . . .	31
Run 2 . . . . .	36
Runs 3 and 4 . . . . .	36
Run 5 . . . . .	40
Runs 6 and 7 . . . . .	40
Run 12 . . . . .	47
Run 14 . . . . .	47
Conclusions . . . . .	55
Recommendations . . . . .	57
Feed Lines . . . . .	57
Injectors . . . . .	58
Combustor . . . . .	58
Appendix A - Fundamentals of Lumped Parameter Equations	60

Table of Contents - continued

Appendix B - Linearized Combustion Delay . . . . .	66
Appendix C - Computer Nomenclature and Model Constants	67
Appendix D - Computer Program . . . . .	76
Nomenclature . . . . .	88
References . . . . .	91

## INTRODUCTION

The work presented in this report was supported by a NASA-MSC contract. It had as its objectives the development of a simulating capability for the LM/RCS, the simulation of the system, and the presentation of a qualitative description of the transient behavior of a preigniter engine.

The Reaction Control System (RCS) for the lunar module (LM) consists of two systems each containing eight engines. The two systems are separate but may be inter-connected by opening cross-feed valves. A cluster of four engines, two from each system, is located at each of four points on the extremities of the vehicle as shown in Figure 1. A schematic of the gas pressurized bi-propellant feed system is shown in Figure 2. As indicated by observation of these figures, the distances between the various engines and their propellant supply source varies appreciably.

The configuration of the LM-RCS engines and their feed supply systems is responsible for hydraulic characteristics capable of severely altering engine performance. Rapid operation of the solenoid-engine injector valves (shown in Figure 3) generates elastic waves in the propellant flow. The hypergolic propellants--the fuel is a blend of hydrazine ( $N_2H_4$ ) and unsymmetrical dimethyl hydrazine  $[(CH_3)_2(NNH_2)]$ ; the oxidizer is nitrogen tetroxide ( $N_2O_4$ )--have different wave propagation velocities. Thus, hydraulic oscillation in the fuel lines have different frequencies from those in the oxidizer lines. The

# LUNAR MODULE - RCS

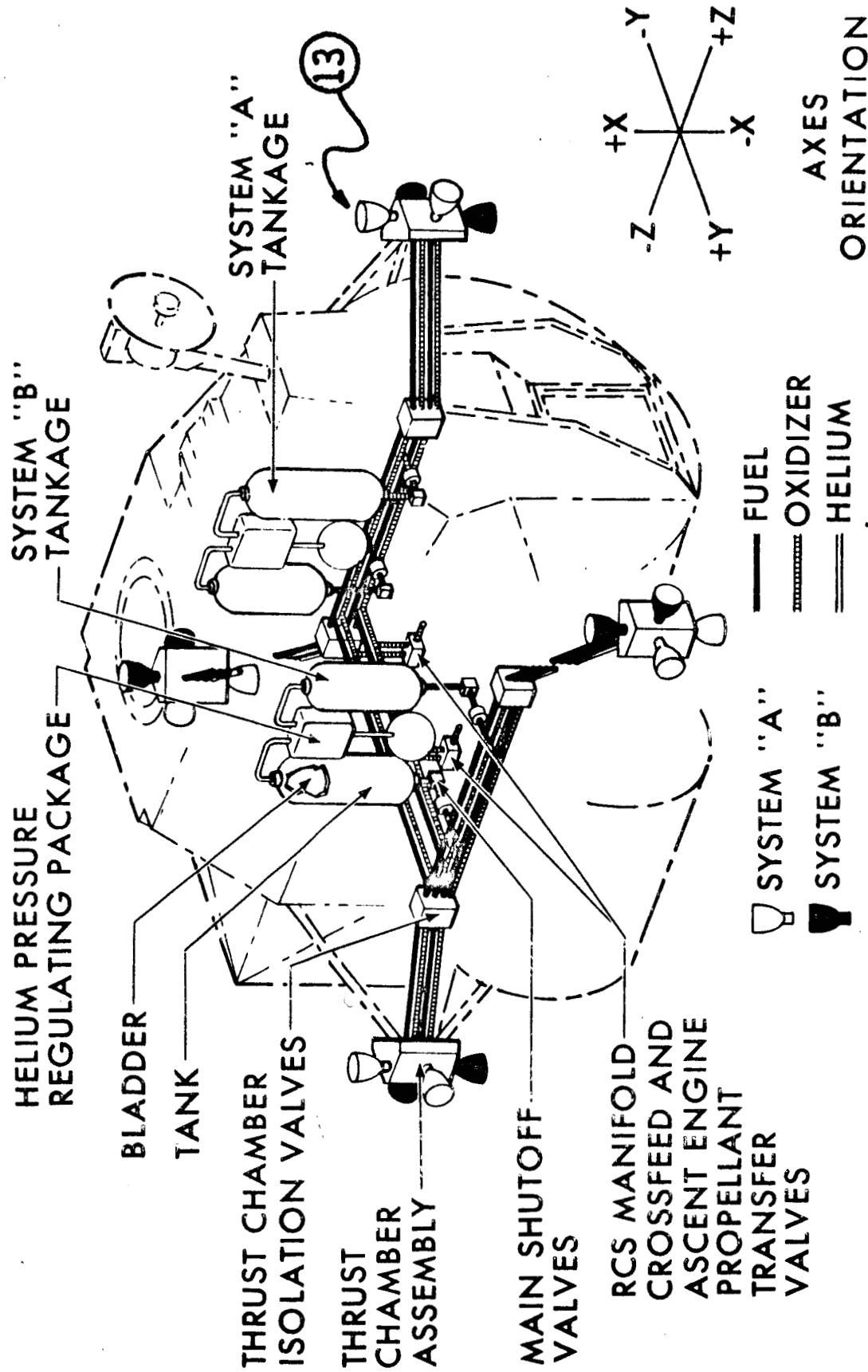
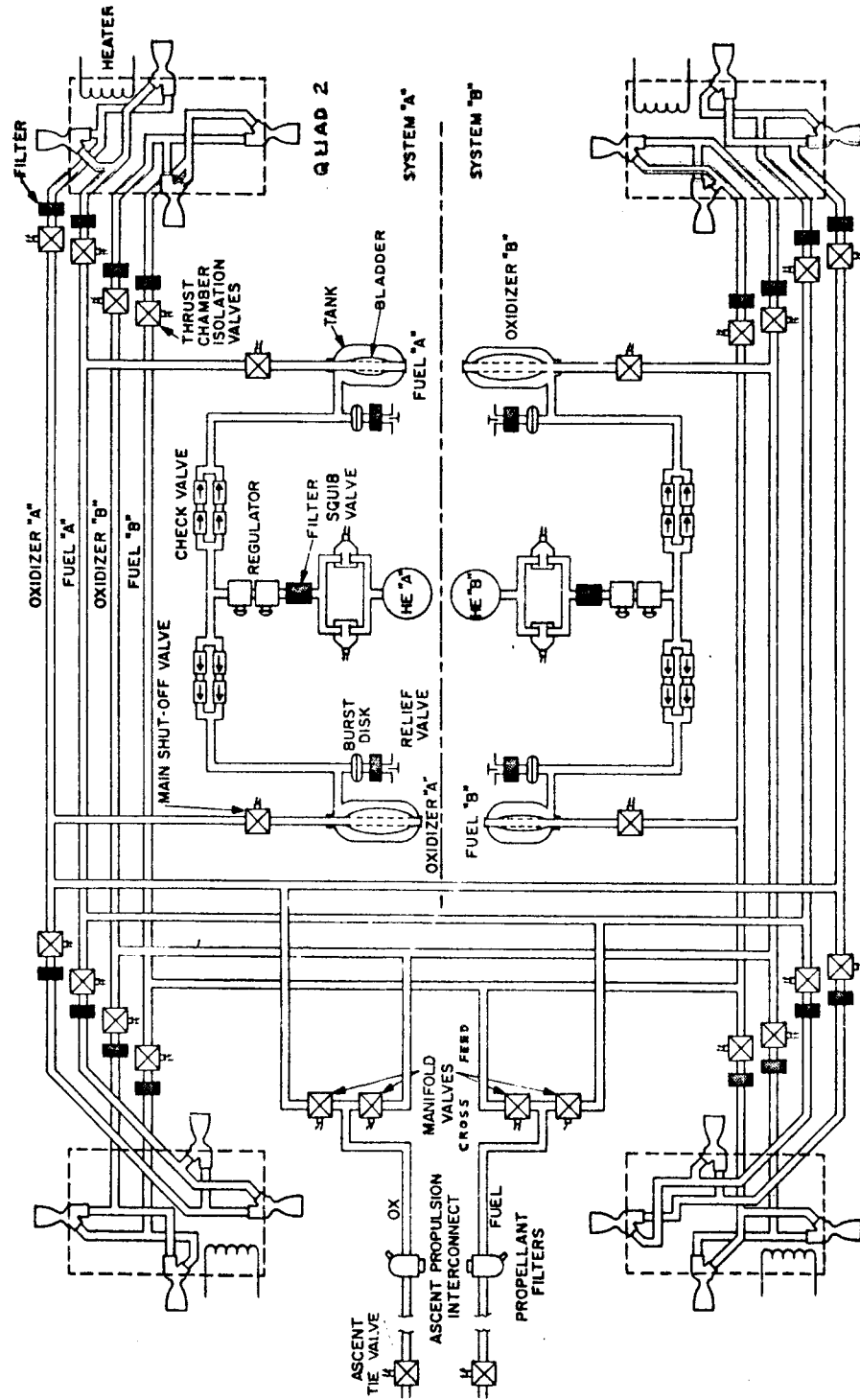


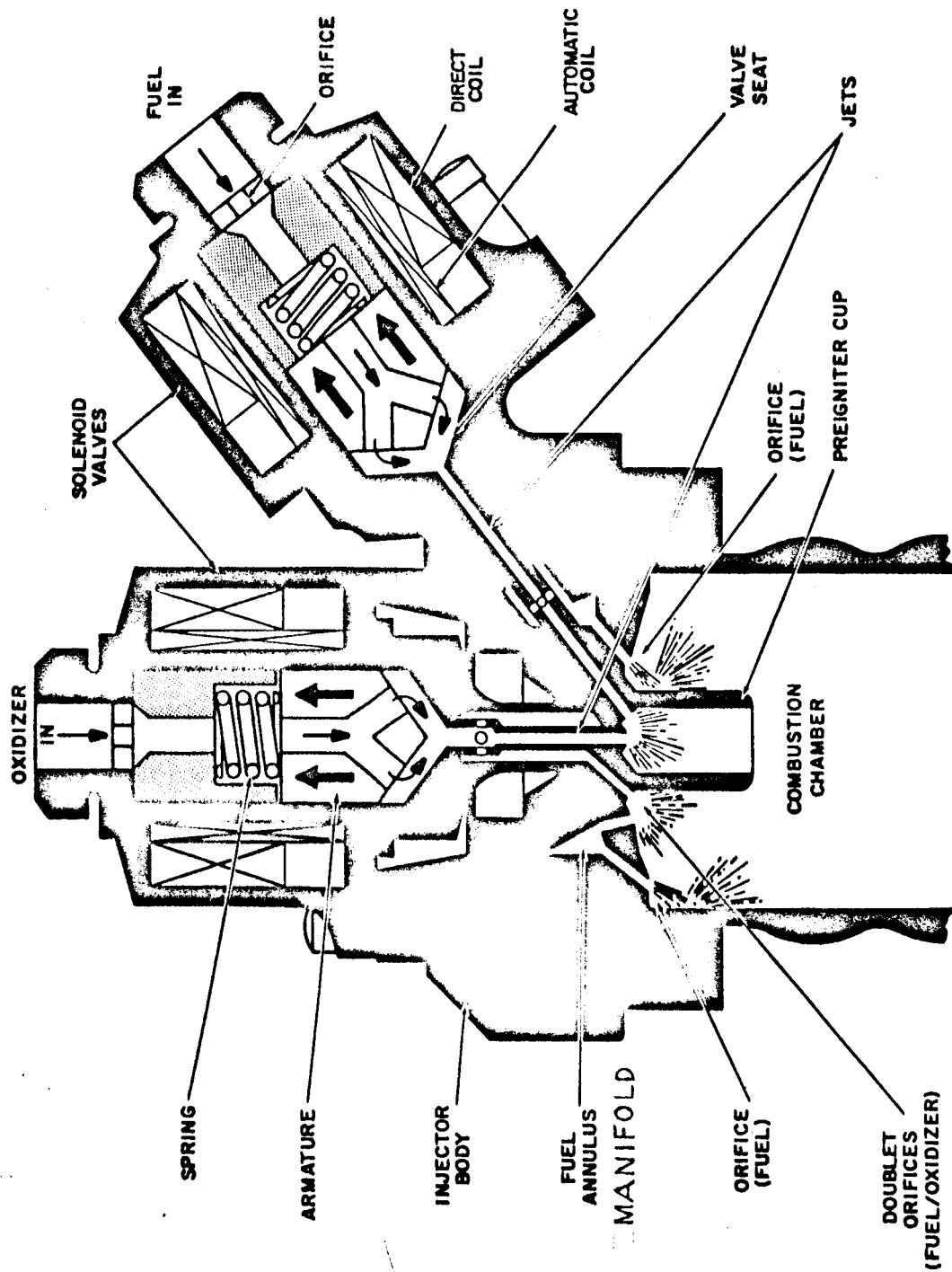
FIGURE 1



RCS PROPELLANT SYSTEM

FIGURE 2





RCS INJECTOR AND VALVES

FIGURE 3

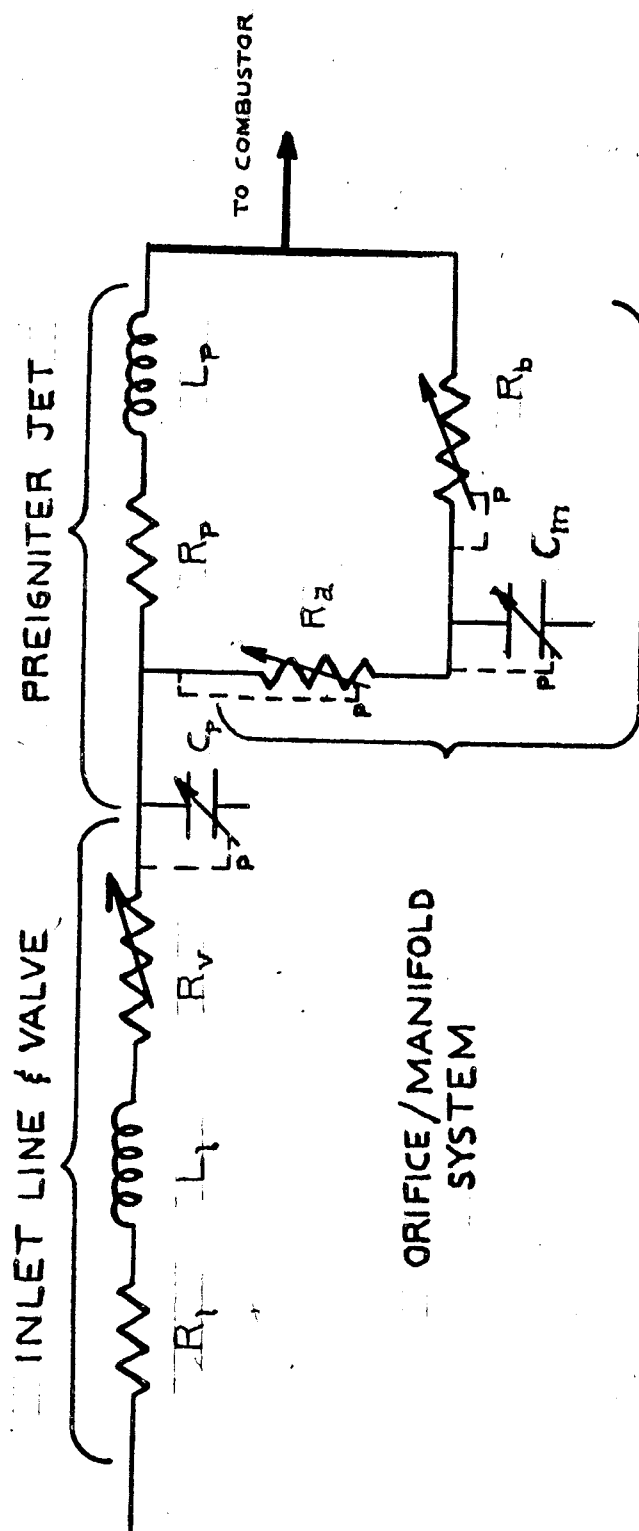
result is that hydraulic transients produce variable oxidizer to fuel ratios. In addition, flow in the various passages of the injector--to the pre-igniter cup and through the manifold leading to the main injector orificies as shown in Figure 3--is in at least two phases immediately after valve opening and following valve closure. These flows in the internal passages of the injector are coupled to the thermochemical processes in the combustion chamber at all time as well as to the oscillating feed system flows when the engine valves are opened. The manner in which this coupling contributes to the extreme chamber over-pressures (ignition spike phenomena, Reference 1) which have been observed (and are in some cases catastrophic) is unknown, but it is certainly significant. These engines are required to operate thousands of times for variable durations as short as ten milliseconds, both in phase and out of phase with other engines.

In an attempt to study some of the above mentioned behavior an analytical program was sponsored by Grumman Aircraft Engineering Corporation, the system contractor. The study was performed by the Advanced Technology Laboratories of General Electric Company. The final report of this investigation was made in March, 1965, (Reference 2). The study indicated that the feed system produced undesirable engine performance. Undesirable performance was verified in pre-production feed-system tests. The study did not include the present injector configuration. Although the study was considered to be based on a full range dynamic model, no allowance was made for the existence of

propellant vapor.

As an ASEE-NASA Summer Faculty Fellow, the present investigator developed a mathematical model allowing for the internal configuration of the injector and more closely representing the physical processes occurring in it. Figure 4 shows this new injector model in terms of electrical equivalents for the various fluid flow elements. The essential characteristic of the elements in this injector was that the flow resistance of the orifices and the capacitance of the fluid accumulating cavities were pressure dependent. The pressure was compared with the propellant vapor pressure to determine the phase of the fluid.

A combination of the new injector model, a feed-system model of the type used by General Electric and a version of General Electric's combustor model up-dated by Grumman RCS personnel was submitted for programming to personnel of the hybrid computing facility at the Manned Spacecraft Center. The programmed material was to provide a simulation of a RCS thermochemical test facility for the purpose of comparing the computer simulation with measured data from the facility. The contract was for the purpose of rendering guidance, evaluation, any necessary modification, and, ultimately, utilization of the computation effort for simulating an actual LM-RCS system. The computing efforts were unsatisfactory for over a year and a half. This eliminated any possibility for modification and utilization of the simulation. In order to achieve a reasonable time scaling in the hybrid computer, the fluid phase changing capability of the model coupled with digital-analog interconnect



L/M-RCS INJECTOR MODEL

FIGURE 4

errors produced instabilities in the computation.

In an effort to obtain some evaluation of the model, an all digital program was written and executed on the CDC 3300 computer of the Lamar Research Center. The computation time required for an all digital simulation being much larger than that required for a hybrid simulation necessitated shorter simulation runs. Since the initiation of the computation effort, experimental data for an actual LM-RCS system firing under vacuum conditions became available at MSC. In view of the two factors mentioned above, it was decided to employ an approximate model of the LM system by using the less complex computation model previously developed for the thermochemical test facility. This required that only one active engine be allowed. It was reasoned that the best model approximation could be obtained by letting the active engine be a system "A" engine located in quad 2 (thus, engine 13 was represented as the active engine of the model). It should be noted that by employing this technique large parts of the feed system were lumped and treated as individual elements. This report presents the results and conclusions drawn from this computation effort.

## METHOD OF ANALYSIS

Feed System

The equations governing the flow of propellant in the feed system are: The non-linear partial differential equations of fluid mechanics or their integrals, thermodynamic and state equations, and the elasticity equations of the propellant piping. The most recent techniques for treating these equations with digital computers for transient liquids and liquids with entrained inert gas are presented and discussed in Reference 3. Conventional methods of analytical treatment and reduction to forms suitable for analog computers are in References 4 and 5.

In the present liquid feed system analysis isothermal quasistatic conditions are assumed; the liquid bulk modulus was considered constant as was that of pressurant gas when entrained in the liquid; and the thin-walled cylindrical pressure vessel equation was presumed to represent the elastic behavior of the piping. The friction-joint method of concentrating fluid friction effects in the form of a Darcy-Weisback pressure drop relation at regular intervals along the flow conduit was utilized (Reference 4). The velocities in regions between friction joints were considered to be small in comparison to fluid accelerations. The equations describing the flow in these regions then reduce to a pair of equations whose solutions can be generated from solutions of the classical one-dimensional wave equations (Reference 4). For sufficiently small regions (i.e., for a large enough number of friction joints distributed

over the system so that they are closely spaced), the assumption of uniform time derivatives is permitted and allows the equations to be written in lumped form similar to those of lumped capacitive and inductive electrical elements. These methods were utilized in the General Electric Study as well as in this study. Their development is included in Appendix A and their use is outlined below.

The first step of the technique for lumping parameters in a fluid system is the division of the system into regions. The regions are separated by friction joints. All friction in a region is represented by a Darcy-Weisback friction factor and equivalent length. The frictional effects of all friction sources are then concentrated at the friction joints on the boundaries of the region. The fraction of the total friction concentrated at each joint is weighted according to the equivalent distance from the friction source to the opposite friction joint. Thus, due to  $N$  friction sources in a region of total equivalent length  $l_e$ , pipe friction factor  $f$ , and pipe diameter  $D$  the magnitude of the pressure drop due to friction which is concentrated at each of two friction joints located at  $x_e = 0$  and  $x_e = l_e$  is respectively

$$(1) \quad \Delta P|_{x_e=0} = \frac{f}{D} \sum_{k=1}^n (l_e)_k \left[ \frac{l_e - (x_e)_k}{l_e} \right] \frac{\rho V^2}{2}$$

and

$$(2) \quad \Delta P|_{x_e=l_e} = \frac{f}{D} \sum_{k=1}^n (l_e)_k \left[ \frac{(x_e)_k}{l_e} \right] \frac{\rho V^2}{2}$$

where  $\rho$  is the fluid density,  $(x_e)_k$  is the average equivalent

distance of the  $k^{\text{th}}$  friction source from the friction joint at  $x_e = 0$ , and  $(l_e)_k$  is the equivalent length of the  $k^{\text{th}}$  friction source; i.e.,  $l_e = \sum_{k=1}^n (l_e)_k$ . Once the friction has been concentrated at the appropriate friction joint, the flow in the interior region is considered frictionless.

In this report, the region of feed line between two adjacent friction joints is referred to as a line module. Two line modules were used in this study. If the flow within a line module were actually frictionless, it would be described by the classical wave equation. Denoting the velocity of propagation of a wave created by any disturbance in the region by "a", the classical theory allows the wave to propagate back and forth through the region with a frequency of  $a/4l$  where  $l$  is the length of the region. When lumping parameters in a fluid line, as was done in this analysis, excitation frequencies in the order of twice the natural frequency of the module can be allowed; i.e.,  $2 a/4l = a/2l$  (Reference 2). The total length of the thermochemical test facility feed line that was to be simulated was approximately 5 feet. This simulation would have allowed disturbing frequency modes of about 600 Hertz(cycles /sec). When the same lumped elements were used to represent the LM-RCS, the module containing the three clusters of non-firing engines had a line branch over fifteen feet long. Hence, this module should have responded to frequency modes up to about 100 Hertz. If one considers a 10 millisecond pulse to be a disturbance of 20 millisecond fundamental period, then the fundamental mode of this disturbance



has a frequency of 50 Hertz. Thus, the 100 Hertz limitation of the simulation renders the response to the second harmonic questionable and the response to modes of higher frequency unacceptable for a 10 millisecond pulse. Nevertheless, 10 m.s. pulses were used for computational economy since the fundamental was represented in the larger module and at least relative effects of disturbing modes of higher frequency would be reflected in other modules which were more finely lumped.

The specific form of the equations for the lumped region between two adjacent friction joints is based upon mass and momentum considerations as would be the case if a distributed description were obtained. However, in the lumped description, it is not possible to account for mass and momentum simultaneously at the same point in the module. Mass and momentum are alternately accounted for in a fashion that keeps the module balanced.

When considering mass conservation, allowance is made for fluid entering and leaving the module at different rates; but the mass accumulation permitted by liquid compressibility and pipe elasticity is considered to be uniform in space at a given instant of time; i.e., the pressure is instantaneously uniform. The result is a capacitive effect.

$$(3) \quad \dot{W}_{in} - \dot{W}_{out} = C \frac{dP}{dt}$$

where C, the fluid capacitance, is defined as the ratio of the rate of fluid accumulation to the rate of pressure increase.

In a simple elastic pipe the capacitance is

(4)

$$C = \frac{V}{a^2}$$

where  $V$  is the volume of the module and  $a$  is the acoustic velocity in the fluid. It is given by

(5)

$$a = \sqrt{B_e / \rho}$$

Neglecting the effect of axial stresses in a thin-walled pipe, the equivalent bulk modulus is related to the fluid bulk modulus and the pipe elastic modulus by

(6)

$$\frac{1}{B_e} = \frac{1}{B} + \frac{1}{E(D_o/D_i - 1)}$$

Momentum considerations are based on different pressures at the two ends of the frictionless region producing an acceleration of the fluid in the region such that the flow rate through the region is instantaneously uniform throughout the region. The result of the inertia of the fluid is production of an inductive effect,

(7)

$$\Delta P|_{\text{inertia}} = L \frac{d\dot{w}}{dt}$$

where  $L$  is given by

(8)

$$L = \int \frac{dl}{A}$$

A balanced arrangement of these frictionless lumped elements is conventionally obtained by splitting either the total capacitance or the total inductance of the module into two equal parts and placing them symmetrically on the ends of the element

which is not split. When the friction at the friction joints is attached to the two ends of the frictionless module, one obtains a module of lumped elements capable of representing flow in a region with friction. A friction element is represented by equation 1 or 2 which is more conveniently expressed as

$$(9) \quad \Delta P \Big|_{\text{friction}} = R \dot{W} |\dot{W}|$$

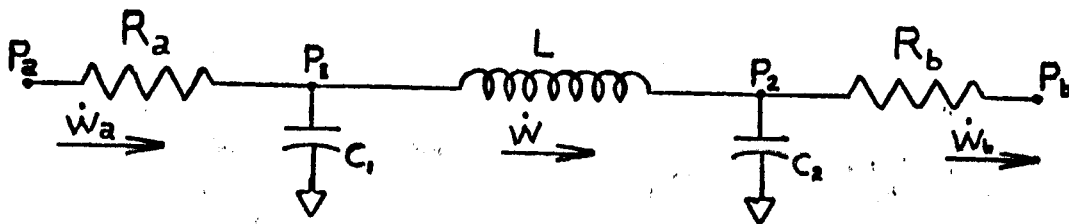
where the velocity has been replaced by its equivalent  $V = \dot{W}/\rho A$  (the absolute value in equation 9 is for keeping track of flow direction) and  $R$  contains the other terms in equation 1, or

$$(10) \quad R = \left| \frac{\Delta P}{\dot{W}^2} \right|_{\text{friction}}$$

With each element now described in terms which are analogous to non-linear electrical circuit elements, the entire module can be represented as a two-port (four-terminal) network. Network equivalents for the two types of modules--split capacitance module and split inductance module--are shown in Figures 5 and 6. The equations for the elements of the modules are also indicated in the figures. By combining the equations of the module elements, a pair of network differential equations may be obtained for each module. The resulting equations implicitly contain pressures as output and flow rates as input for the split capacitance module. For the split inductance module, the converse is the case as the outputs are flow rates for input pressures. This characteristic is utilized in selecting one of the two types of modules.

Propellant supply tank pressures were treated as known

### SPLIT CAPACITANCE LINE MODULE



$$P_a - P_1 = R_a \dot{W}_a |\dot{W}_a|$$

$$C_1 \frac{dP_1}{dt} = \dot{W}_a - \dot{W}$$

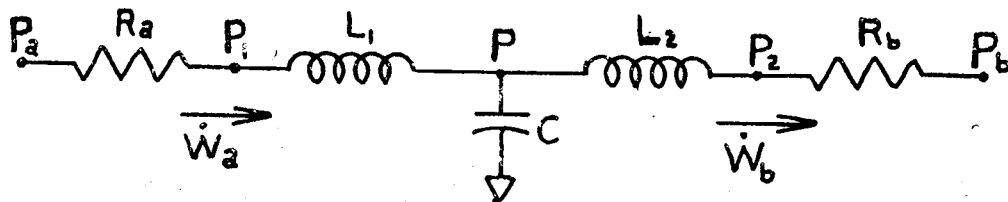
$$P_1 - P_2 = L \frac{d\dot{W}}{dt}$$

$$C_2 \frac{dP_2}{dt} = \dot{W} - \dot{W}_b$$

$$P_2 - P_b = R_b \dot{W}_b |\dot{W}_b|$$

FIGURE 5

### SPLIT INDUCTANCE LINE MODULE



$$P_a - P_1 = R_a \dot{W}_a |\dot{W}_a|$$

$$P_1 - P = L_1 \frac{d\dot{W}_a}{dt}$$

$$C \frac{dP}{dt} = \dot{W}_a - \dot{W}_b$$

$$P - P_2 = L_2 \frac{d\dot{W}_b}{dt}$$

$$P_2 - P_b = R_b \dot{W}_b |\dot{W}_b|$$

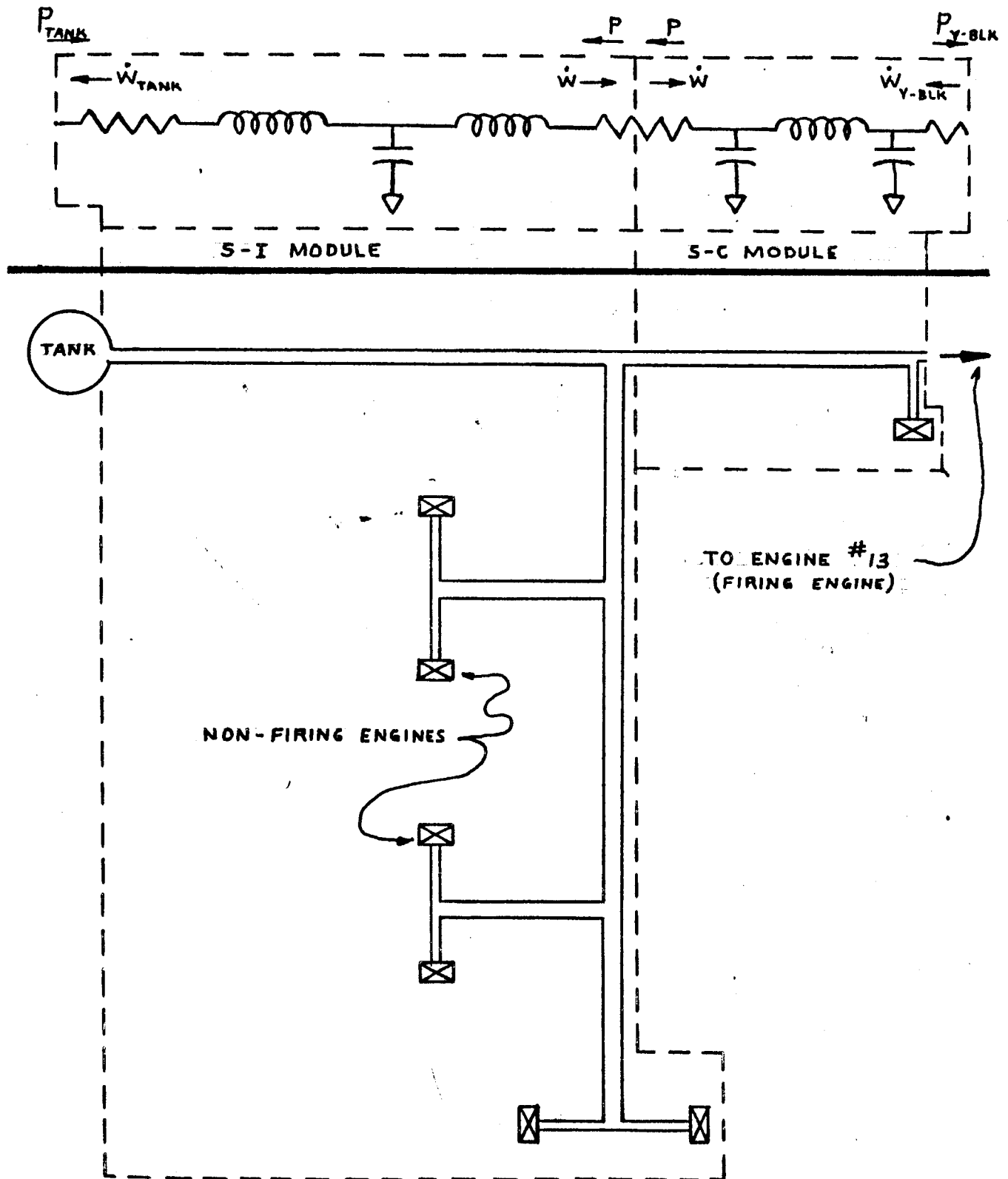
FIGURE 6

constants in the present analysis. With this information as input, a split inductance line module connected to the tank represented the feed line leaving the tank. The outputs on both ends of this module were flow rates. Thus, a split capacitance line module represented the next lumped region of feed system piping. This module utilized as input the output flow rate of the split inductance module. Its output was the pressure required for the input of the split inductance module. These two modules for the LM-RCS represented the entire 5/8-inch diameter feed line to the Y-block of the firing engine as well as all feed lines to non-firing engines. The 3/8-inch diameter line from the Y-block to the firing engine was considered to be part of the injector inlet for the firing engine (Engine #13). A schematic representation of one propellant feed system is shown in Figure 7 with arrows indicating input and output information for each module.

### Injectors

The equations for the basic liquid flow elements in a single pipe line were presented in the preceeding discussion of the feed system. The elements can be classified as resistors (friction elements), capacitors (mass accumulating elements), and inductors (mass inertia elements). A resistor was represented by Equation 9. The description of a capacitor was given in Equation 3. Equation 7 gives the relation for an inductor. For the injector, the same ideas can be used, but due to fluid phase changes a more complex interpretation must be applied.

Modules for a flow device may be constructed by combining



FEED LINE MODULES REPRESENTING LM-RCS SYSTEM

FIGURE 7

the elements so that the steady flow relation between pressure drop and flow rate determines the resistance,  $R$ ; transient pressure drop due to inertia determines the inductance,  $L$ ; and the mass accumulating characteristics of the device determines the capacitance,  $C$ . If the flow device is complex, the parameters,  $R$ ,  $L$ , and  $C$  will probably be non-linear (i.e., they will depend upon  $P$  and/or  $W$ ). Such a procedure for representing flow devices, particularly as a schematic representation of the device, may be of great convenience but is purely artificial and only as good as has been the consideration of the actual physical processes. As the engine injectors of this study are complex flow devices, the resistive, inductive, and capacitive elements may be of the above mentioned non-linear type.

A schematic diagram of an injector for this study is shown in Figure 4. Because an inlet line to the injector is only 3/8 inch in diameter and 10 inches in length, its capacitance is negligible. Thus, an inlet line has only inductance,  $L_i$ , and resistance,  $R_i$ . In addition to the line resistance, the inlet valve is represented by a time variable resistor  $R_v$ . Downstream from the valve, the fluid fills the tube leading to the preigniter cup. (See Figure 3). In addition to some fluid flowing out the preigniter into the chamber, most of the fluid flows through a parallel branch into the injector manifold feeding the main injector orifices. The dribble volume of the injector--the volume of propellant which can be trapped in the cavity between the valve and the chamber--is composed of the volume of the preigniter tube and that of the injector manifold.

Since accumulation occurs in the dribble volume regions during start-up and depletion during tail-off, they are represented by capacitors. However, in the actual computer calculations, the preigniter capacitor  $C_p$  was omitted since its capacity was an order of magnitude smaller than that of the manifold during a very short filling period and zero thereafter. The large length to diameter ratio of the preigniter tubes makes their inductance significant and accounts for the constant preigniter inductor,  $L_p$ , shown in the schematic (Figure 4). The orifices between the preigniter tube and the injector manifold are represented by the resistor,  $R_a$ , between the preigniter capacitor,  $C_p$ , and the manifold capacitor  $C_m$ . The resistor,  $R_b$ , between the manifold capacitor and the combustor represents the main injector orifices.

The following discussion applies to the physical processes represented in the elements of the above described injector module. Liquid and vapor phases were considered. All processes in the injector were treated as isothermal and transitions as quasistatic. The propellants were presumed to be at 70°F. The vapor pressure at that temperature was used as the sole criterion determining the phase. For pressures below the vapor pressure, the value of a capacitor was based on its contents being an ideal gas. For pressures above the vapor pressure a capacitor was assumed to contain only liquid propellant. A small liquid volume in a rigid container has a negligible capacitance. When the pressure in a capacitor was equal to the propellant vapor pressure, liquid and vapor phases were considered to coexist, and the



capacitance was unlimited (a Dirac delta function) until the volume contained either all liquid or no liquid. If  $W_L$  is the liquid propellant mass in the cavity when it is full of liquid and  $W_V$  is the vapor propellant mass contained by the cavity when it is full of vapor at the vapor pressure  $P_V$ , then the capacitance of the injector cavity is represented by the following function of cavity pressure:

$$(11) \quad C = \frac{W_V}{P_V} \left[ 1 - U(P - P_V) \right] + (W_L - W_V) \left[ \delta(P - P_V) \right]$$

where  $U$  and  $\delta$  are respectively the unit step function and the Dirac delta function. Substituting this pure function of pressure into the fundamental capacitor equation, Equation 3, results in

$$(12) \quad W_{\text{cavity}} = \int_0^P C dP$$

This integral was evaluated and is shown in Figure 8. The integral in Equation 12 was used as a table in the program for determining cavity pressures. The table look-up was based on net integrated mass flow into a cavity.

The resistor ( $R_a$ ) leading from the preigniter tube to the manifold cavity and the resistor ( $R_b$ ) between the manifold and the combustor were given phase dependent characteristics. For a constant orifice coefficient, the resistance is inversely proportional to fluid density. The gas phase density was estimated as 1/100 of the liquid phase density. Hence, a gas phase resistance of 100 times the liquid phase resistance was used. All liquid phase resistances were based on pressure-drops and flow rates during steady state engine operation.\* The value

\* Obtained from Mr. Doug Sedgley, Reaction Control Section, Grumman Aircraft Engineering Corporation, Bethpage, Long Island, New York.

TWO - PHASE  
CAVITY CAPACITOR  
PRESSURE vs. MASS

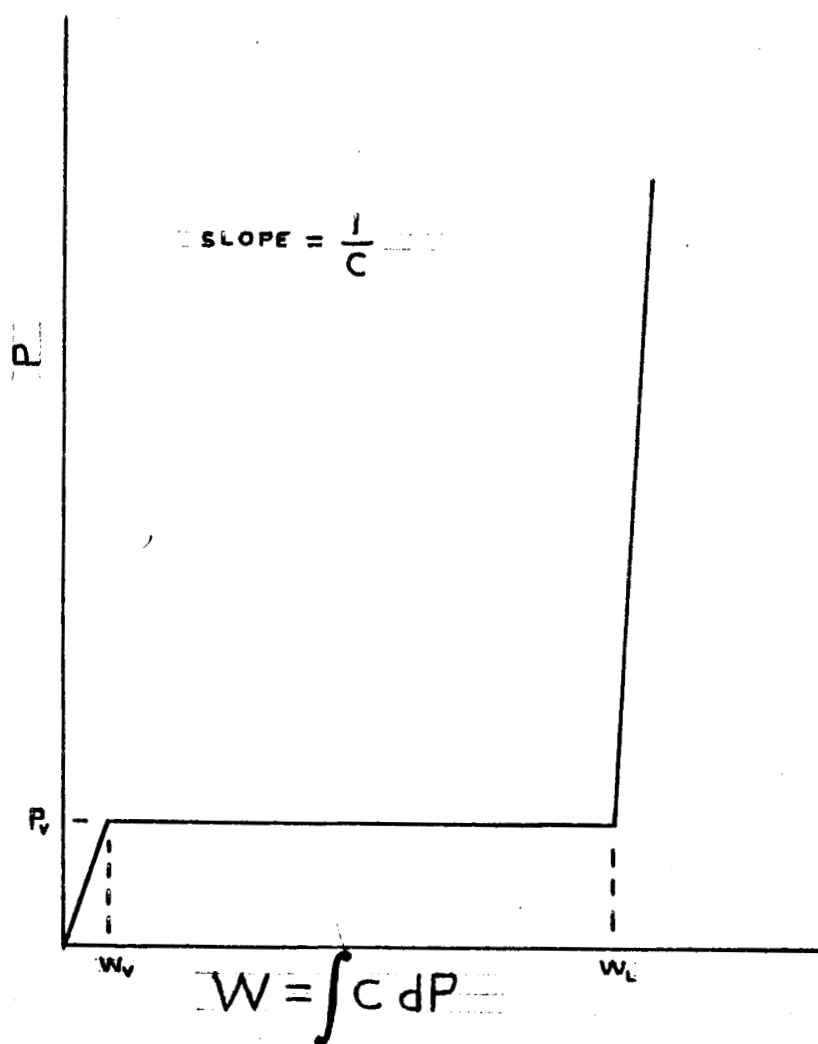


FIGURE 8

of a two-phase resistance was based on the pressure of the upstream capacitor. Thus,  $R_a$  was dependent upon  $P_p$  and  $R_b$  depended upon  $P_m$  (See Figure 4).

Several schemes were investigated for changing the resistance of an orifice when its upstream pressure reached the vapor pressure. The presence of a gravity field on an up-firing engine with quasi-static flow would require that a cavity be completely filled with liquid before allowing liquid to flow through its downstream orifice. In a down-firing engine, an orifice would flow liquid as long as its upstream cavity contained any liquid at all. Essentially, both of these schemes were used. They provide the criteria for changing the phase of the flow through an orifice without simultaneously considering both phases. They also provide two extremes for treating a mechanism which has been experimentally observed to greatly influence tail-off phenomena and the associated generation of spike-inducing intermediates. Computational instabilities associated with the suddenly shifting resistors caused several modifications in the above schemes. One modification was in effect only when the engine valve was open. Under this condition, the resistance  $R_b$  was allowed to decrease linearly with increasing liquid mass in the upstream cavity. Another modification inhibited backflow through the main injector doublets. (The combustor model would treat such flow as replenishing the injector with unburned propellant from the combustor.) An additional modification was the previously mentioned elimination of the preigniter capacitor. With this alteration,  $R_a$  was made

dependent upon the manifold pressure  $P_m$ . For  $P_m$  equal to or greater than the vapor pressure, the liquid value of  $R_a$  was used. Otherwise the gaseous value was employed.

#### Combustor

A slightly modified version of the General Electric Company's combustor model (Reference 2) was employed in this study. The model was based on mass conservation in the combustion chamber. The chamber pressure during combustion was determined by a mass balance on gases generated from the injected liquid propellants and gases escaping through the nozzle. The efflux through the nozzle was determined by the chamber pressure and the characteristic velocity. The characteristic velocity was treated as a pure function of the mixture ratio of propellant generated gases. The propellant gas generation rate was determined from the liquid injection rate retarded by time,  $\tau$ , a variable time delay.

The time  $\tau$  was the time for which propellants were inert during a fictitious process following injection. At time  $\tau$  after injection the process instantly converted propellants into gaseous combustion products having a characteristic velocity dependent upon the propellant mixture ratio at the time of conversion. This fictitious process utilizing the combustion time delay was a simplified way of representing the rate processes of atomization, mixing, evaporation, and reaction. When the controlling rate process is that of vaporization, the model well represents the effects of the chamber processes (Reference 6).

The equation for the combustor pressure was:

TABLE I  
CHARACTERISTIC VELOCITY FOR ANALYTICAL COMBUSTOR MODEL

$R_w$ (Ratio)	$C^*$ - ft/sec
0	0
.2	2925
.4	3450
.6	3985
.8	4450
1.0	4990
1.1	5170
1.2	5300
1.4	5310
1.5	5305
1.6	5260
1.7	5170
1.8	5130
1.9	5070
2.0	4990
2.1	4940
2.2	4900
2.3	4790
2.4	4720
2.5	4640
2.6	4560
2.8	4400
3.0	4230
3.2	4070
3.4	3900
3.6	3710
3.8	3535
4.0	3380
20.0	0

# COMPLETE RCS TEST FACILITY SCHEMATIC

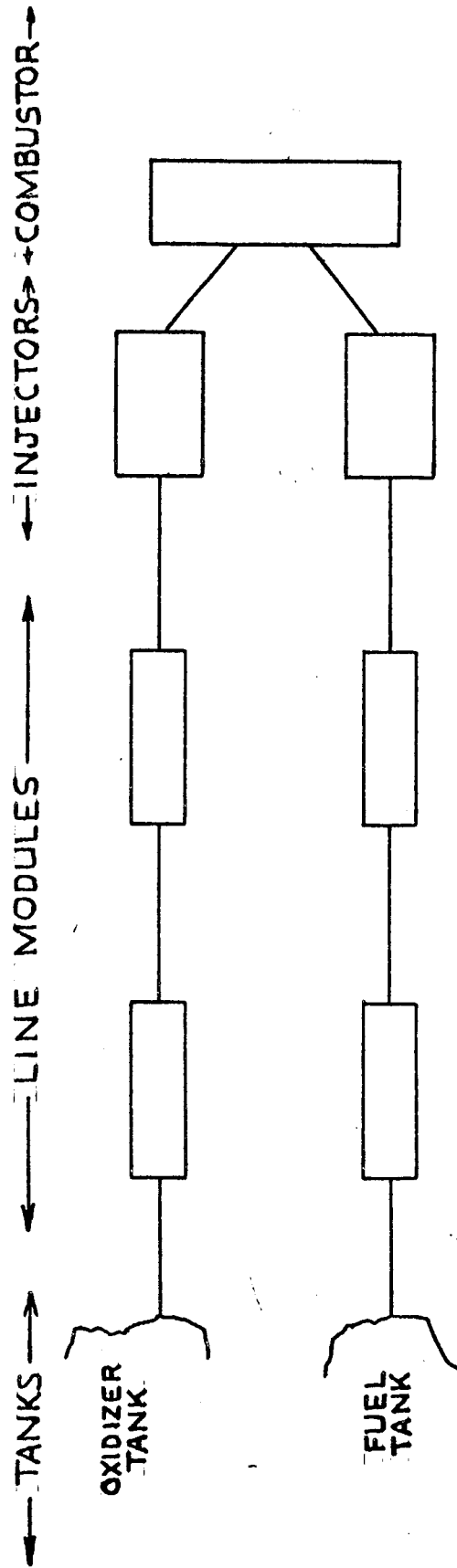


FIGURE 9

oxidizer and the fuel system were each represented by two line modules and an injector module. A tank provided a constant pressure input to a split inductance line module which in turn provided a flow rate input to a split capacitance line module. The downstream pressure output of a split capacitance line module was input for an injector module. The upstream output of the injector module was the flow rate input required on the downstream side of the split capacitance line module. The downstream output of each injector was the flow rate of its propellant. The ratio of these two outputs provided the mixture ratio

$$(17) \quad R_W = \frac{\dot{W}_{Ox}}{\dot{W}_F}$$

and their sum gave

$$(18) \quad \dot{W}_L = \dot{W}_{Ox} + \dot{W}_F$$

These inputs for the combustor model determined chamber pressure which in turn was required as input to the injector module.

The nomenclature and values for model constants for the computer program are presented in Appendix C.

Appendix D contains a logic flow diagram and a listing of the program.

## RESULTS

### Hybrid (Analog-Digital)

This contract required programming and computing to be performed at the MSC. Hybrid techniques were recommended. However, acceptable results were never realized for computations reasonably representative of the model. Although general areas of difficulty could be detected, the complex interconnection systems between the digital and analog computers imposed both random and variably biased errors on the computations which never permitted satisfactory alleviation of the computational difficulties. The results of these attempts are not presented in this report. They are contained and discussed in Reference 7, the final report prepared by the hybrid simulating personnel at MSC.

### Digital

To utilize the excellent error diagnostic capabilities of digital computers, the equations of the system elements were programmed for a CDC 3300 digital computer. After minor modifications, stable computations were achieved. Forward differences with a time step size of 10 microseconds were ultimately employed with complete system data output every 20 steps (each 0.2 milliseconds). This resulted in approximately three milliseconds of reasonably well simulated engine life per minute of digital computer time. This high rate of computer time consumption severely limited the scope of the simulation, but it was necessary for the representation of rapid valve actuation. The speed of these same calculations would have been increased



by a factor of about 20 had more sophisticated computing machinery of the type normally utilized by NASA been employed. Nevertheless, in view of the time consumed by the hybrid computing attempts at MSC and the effort expended in digital programming by the contractor, employment of the above mentioned computing procedure served as verification of the simulation techniques and enabled realization of contract objectives.

Diagnostics of the early digital attempts led to the previously discussed alteration in shifting the injector manifold resistors during the pre-ignition period of operation. Reduction of the main orifice resistors at a rate linearly dependent upon dribble volume liquid content during open injector-valve engine operation produced acceptable stability in the simulation.

The simulation became insensitive to finite difference approximations of rapid transients with the use of 10 micro-second computation intervals.

Extreme backflow occurred through the main injector orifices immediately following chamber ignition. This ignition was caused by flow through the preigniter jets. The single combustor model employed could not distinguish between preigniter and main chamber combustion. Consequently, any backflow was treated as a liquid propellant backflow. This backflow entered the main injector orifices because its dribble volume was not yet filled with liquid. According to the injector model, the dribble volume remained at the propellant vapor pressure. In reality, any backflow from the chamber after ignition would consist essentially of combustion product gas. A very small mass of this gas would

provide appreciable pressurization of the dribble volume preventing further backflow. Since the combustor model in its prevailing form did not allow for product backflow, this physical condition was more closely approximated in the model by inhibiting the backflow through the main injector. The resulting characteristic ignition transient in the simulated chamber pressure is compared with experimental data in two cases (runs 1 and 3). The general characteristics of the results are very good for a first computing success with the model.

Fifteen simulated test runs were planned, and their required data input were prepared. As computing time became critical several of the less interesting runs were aborted. Manual plotting of all of the huge quantity of output from the runs would have been prohibitive. Selected results representative of the simulation were plotted and are included in this report in Figures 10 through 27.

All figures have a common abscissa of time--10 milliseconds per inch--starting from the beginning of the first valve opening motion. Each valve was assumed to travel its full stroke (at constant velocity) in 1.5 milliseconds. Periods from the beginning of valve opening until the completion of valve closure are indicated on the chamber pressure plots for each run by F-valve for open fuel valve and O-valve for open oxidizer valve. The boundaries of the open fuel valve periods are vertical solid lines on all figures. Similarly, vertical dashed lines indicate the boundaries of periods during which the oxidizer valve was open.

Discussion pointing out inadequate details of the plotted results follows:

Runs 1 and 15

Run Number 1 represents a single 12 millisecond nominal duration pulse. The fuel valve led the oxidizer valve by 2 m.s. during opening and it led 0.7 m.s. during closure. Propellants were considered pure. The injector resistors shifted in the manner simulating an up-firing engine attitude during the tail-off period following closure of the valves.

The two peaks in the chamber pressure of Figure 10 are due to preigniter ignition--23 psi--and the reaction following the commencement of main doublet liquid flow--110 psi. At the completion of fuel valve closure, the pressure falls sharply to a near zero value. The simulating engine then "chugs" at 5 to 10 psi levels for the remainder of the run. This "chugging" is due to the vapor pressure of the propellants driving the propellant into the combustion chamber.

Plotted on the same chamber pressure graph--dark dashed curve--are experimental data from an actual 14 m.s. pulse of Engine 13 (data from a 12 m.s. pulse was not available). It is easily seen that pressure fluctuations in the actual engine are not as abrupt as those of the model.

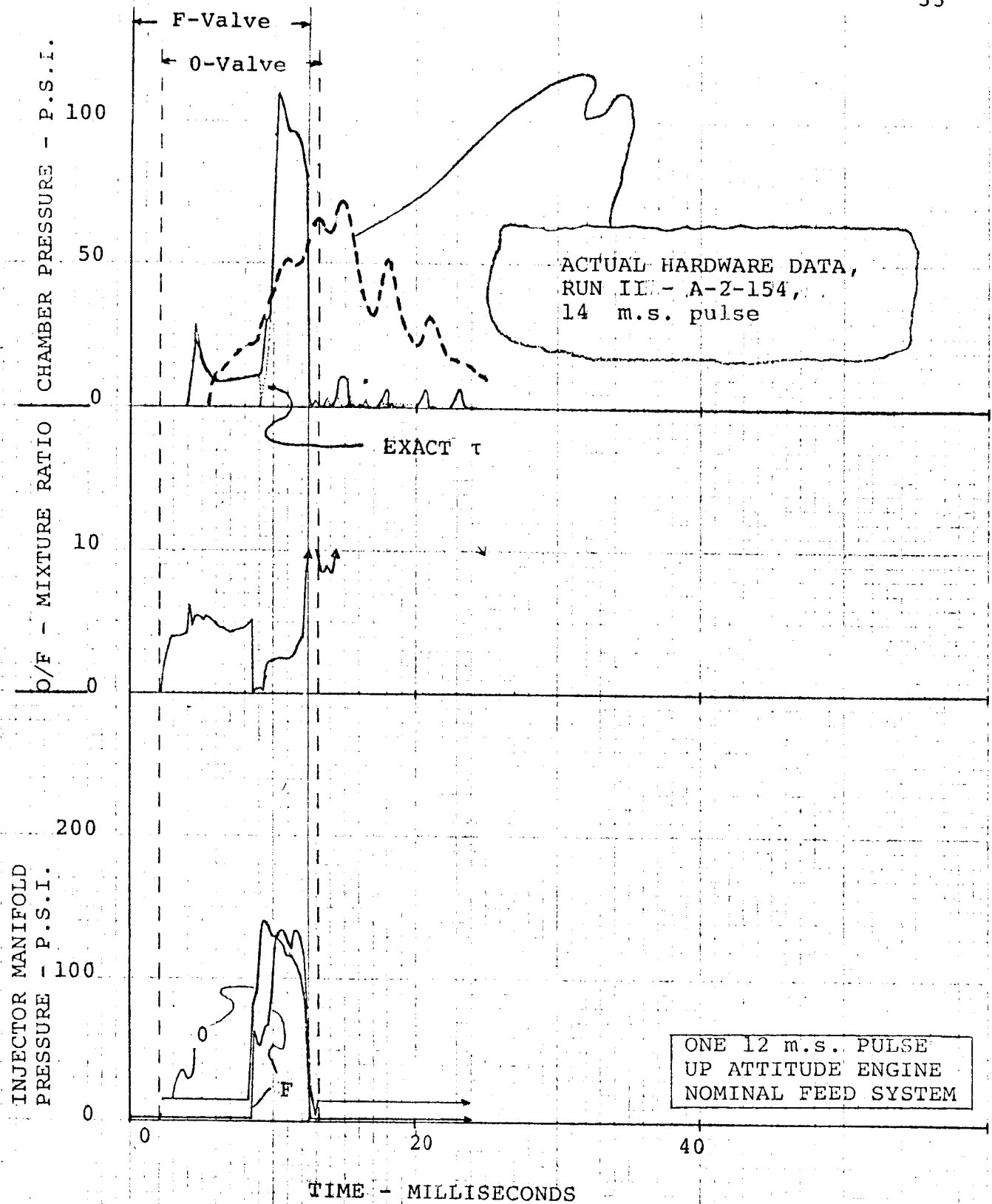
All runs except run 15 were performed with the linearized combustion delay time ( $\tau$ ) model for improved calculation efficiency. Run 15 duplicated run 1 but used the forward differences to solve the differential equation for  $\tau$ . Only

minor differences were observed during some of the severe fluctuations. The chamber pressure results of run 15 are plotted as a fine dotted curve superimposed on the results of run 1.

The oxidizer to fuel mixture ratio of run 1 is also shown in Figure 10. Values greater than 10 were not plotted. The mixture ratio is high--around 5--during dribble volume filling when the only liquid injection is due to preigniter flow.

Pressures in both the fuel and the oxidizer injector manifold dribble volumes are also presented in Figure 10. Figure 11 presents Run 1 pressures at three locations in each propellant feed system. The top graph of the figure is for a location just downstream of the valve in the preigniter tube. The middle graph gives pressures on the upstream side of the valve, and the lower graph presents those at the Y-block. A sharp maximum feed line pressure of 370 psi occurs on the upstream side of the oxidizer valve at the time of complete valve closure. This is followed by smooth maxima of 285 psi in both the upstream valve position and the Y-block position which is more indicative of actual system behavior due to its location in the feed line module. Severe derivatives in the neighborhood of a maximum at the valve location would indicate wave generation activity, but high precision in the indicated intensity would not be expected.

Mass flow rates at four locations in each stream are shown in Figure 12. Note that the ordinate readings, in pounds per



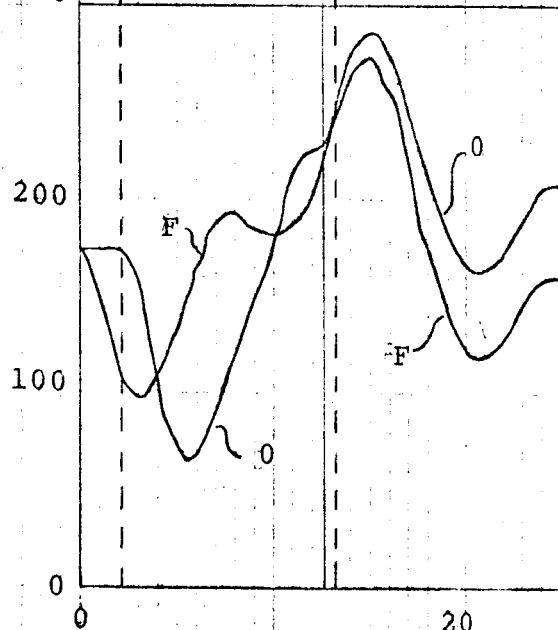
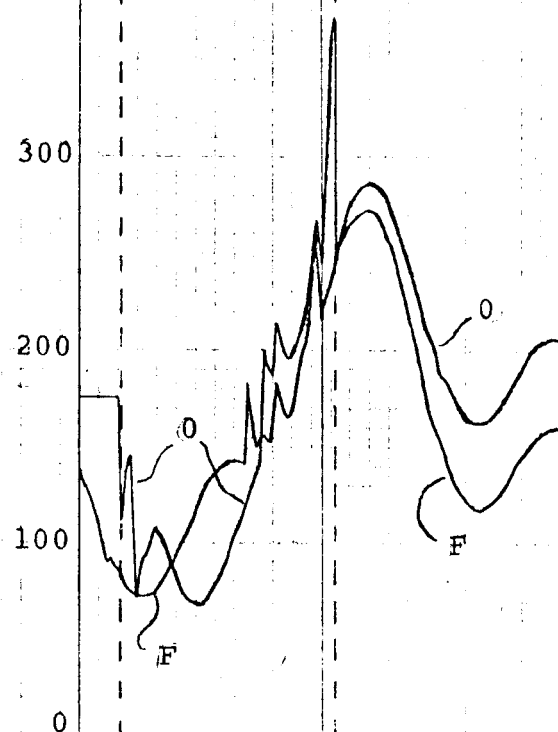
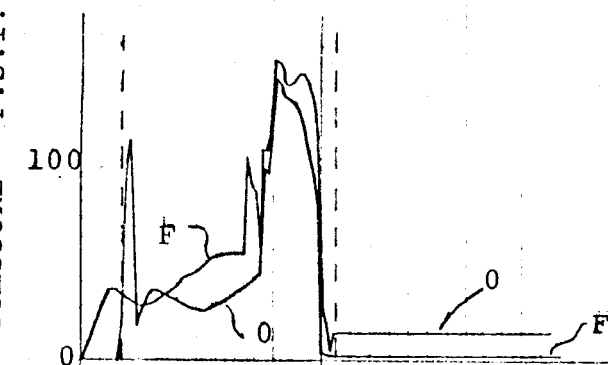
RUN - 1

Figure 10

PREIGNITER INJECTOR  
PRESSURE - P.S.I.

UPSTREAM VALVE PRESSURE - P.S.I.

Y-BLOCK PRESSURE - PSI



ONE 12 m.s. PULSE  
UP ATTITUDE ENGINE  
NOMINAL FEED SYSTEM

TIME - MILLISECONDS

RUN - 1

Figure 11

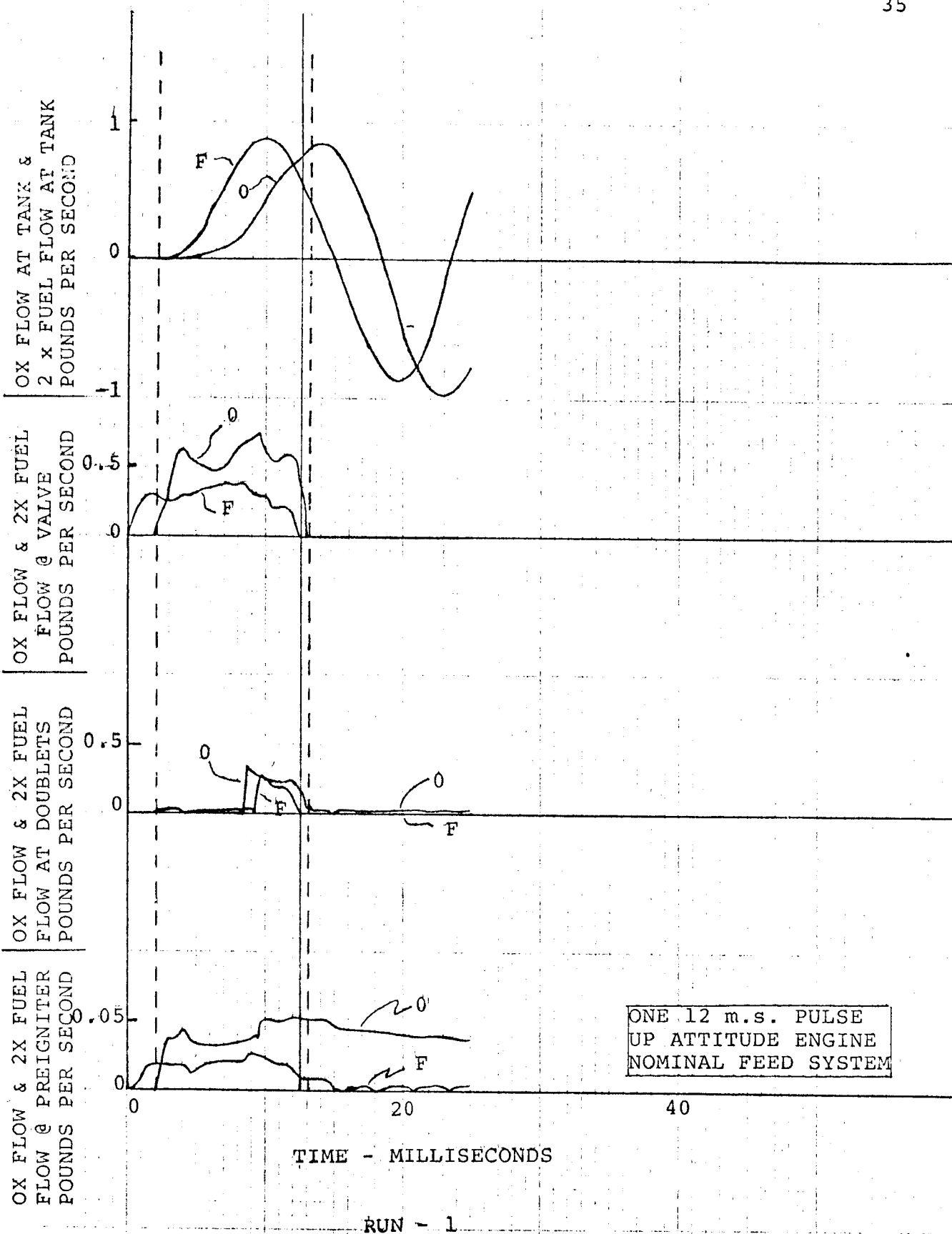


Figure 12

second, apply only to the oxidizer flow. An ordinate reading must be divided by a factor of two before it applies to a fuel reading. This was done because of the design mixture ratio being 2.0. The top three graphs pertain to the main propellant flow respectively at the tanks, the valves, and the main injector doublets. Their scale is one pound per second per inch for oxidizer or 0.5 pounds per second per inch for fuel. The lower graph pertains to the preigniter flow and its scale is only one tenth that of the other mass flow rate graphs.

#### Run 2

Run 2 was identical to run 1 except a down-firing engine attitude was represented during the tail-off period.

The only results presented for this run are in Figure 13. The figure contains chamber pressure, mixture ratio, and dribble volume pressure. Note that due to faster dribble volume emptying the tail-off "chugging" is more intense than that for the up-firing engine. This is in qualitative agreement with engine test results.

#### Runs 3 and 4

Runs 3 and 4 represent firings of nominal 40 m.s. pulse width. Run 3 is for an up-firing attitude and run 4 is for a down-firing attitude. Run 4 was terminated shortly after valve closure.

The only results presented (Figures 14 and 15) are those of chamber pressure, mixture ratio, and dribble volume pressure. However, experimental data from a 50 m.s. pulse is compared with the chamber pressure of run 3. Again the actual engine



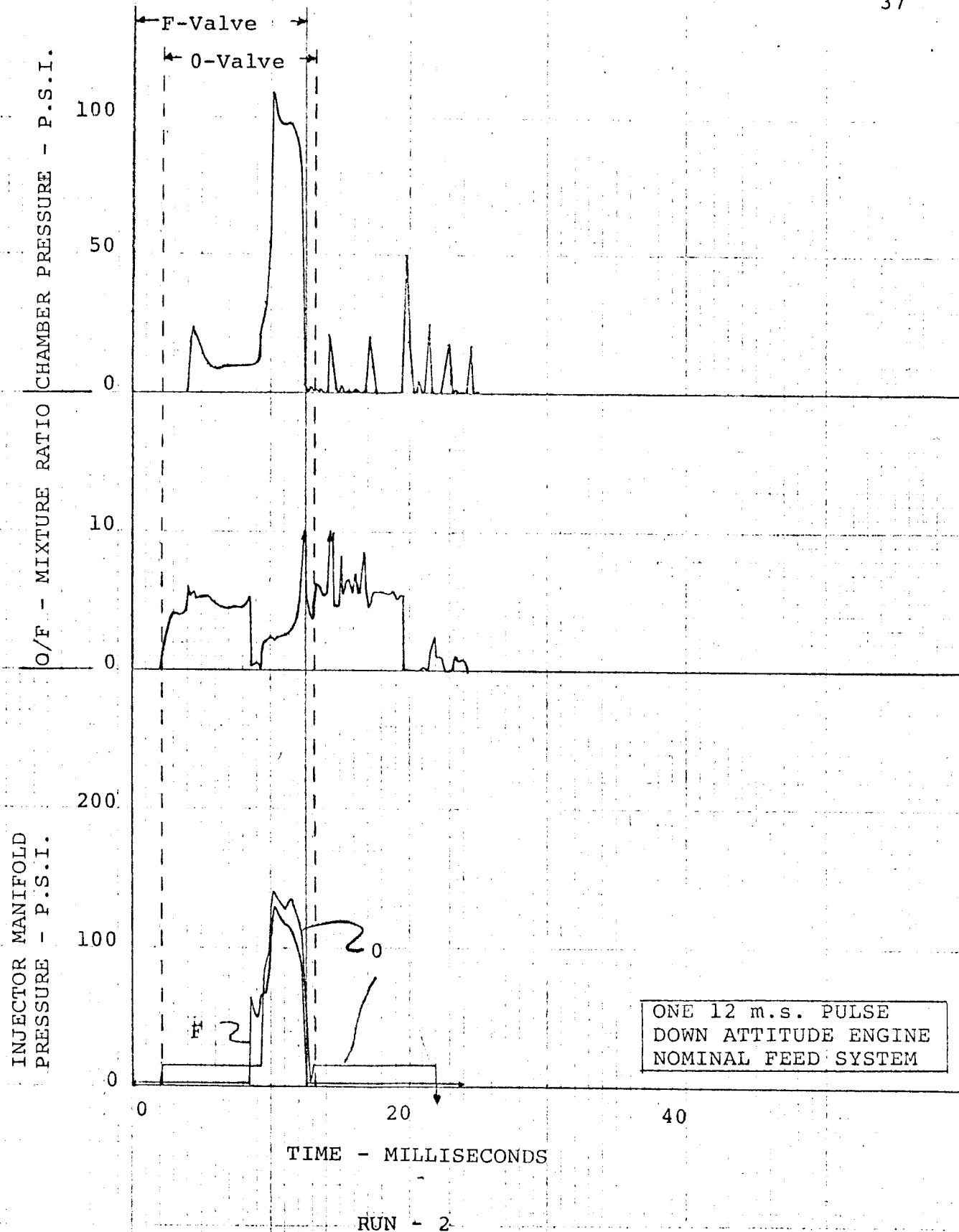


Figure 13

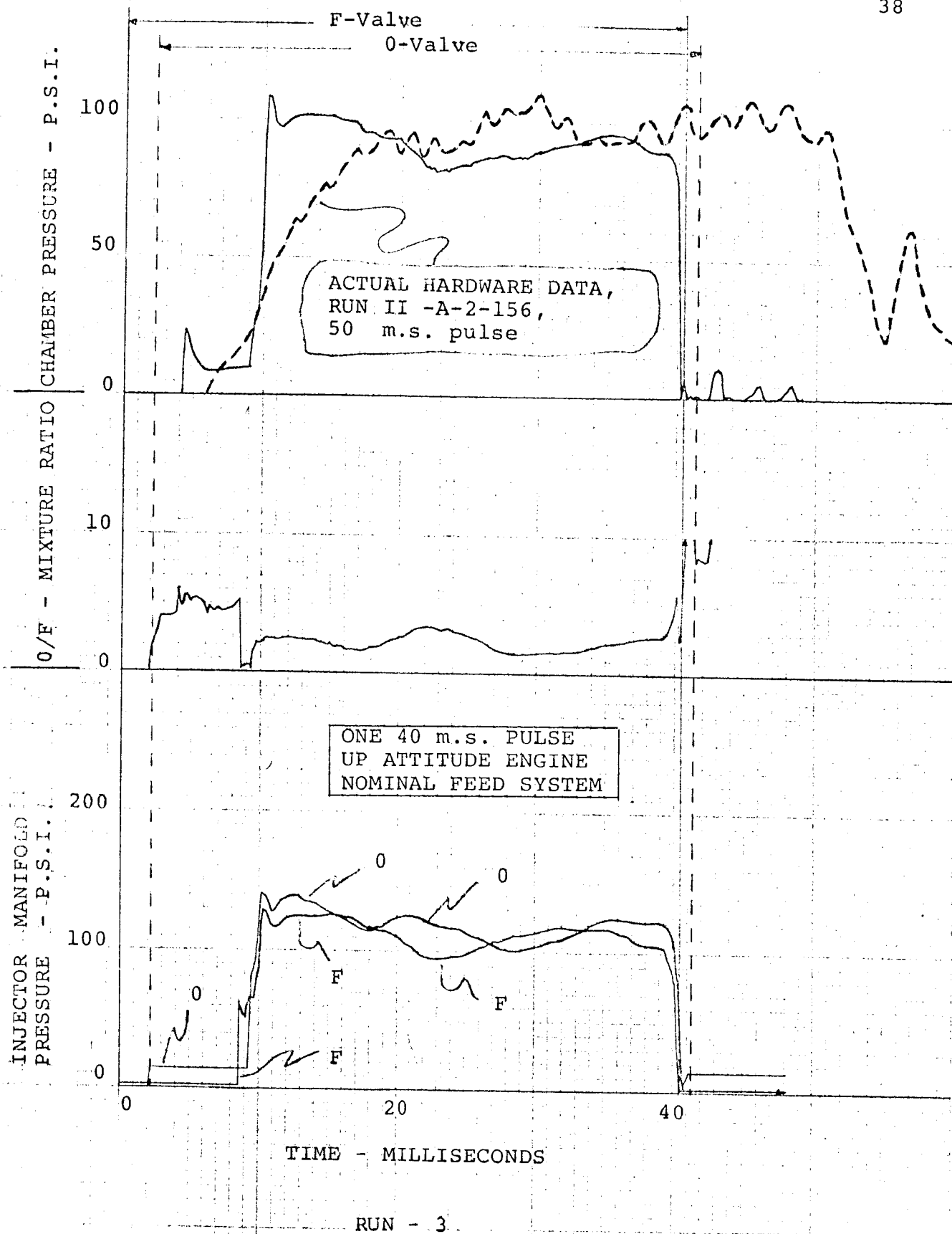


Figure 14

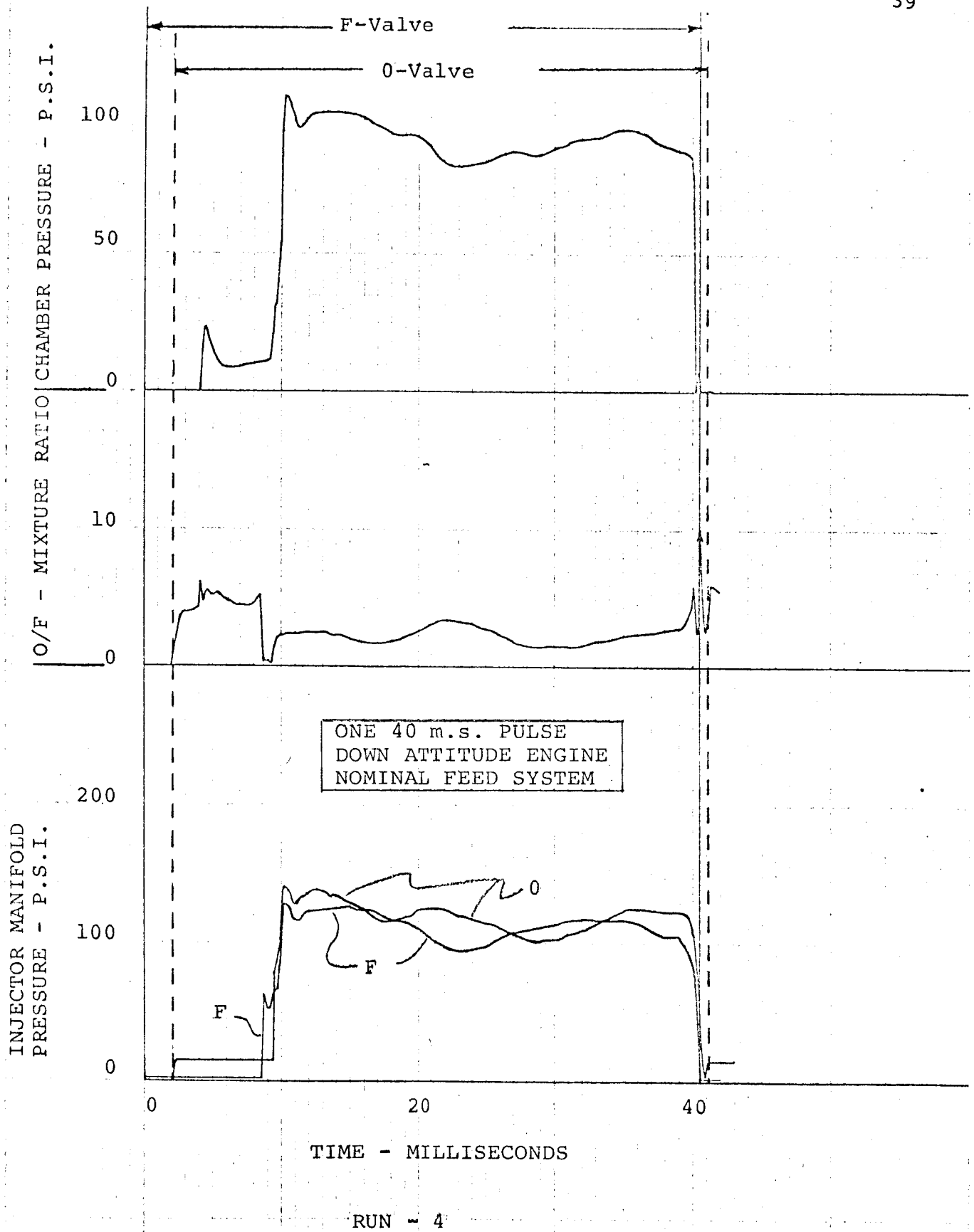


Figure 15

pressure transitions are not as abrupt as those of the model.

A significant observation is that of chamber pressure frequency. Both experimental and model data have a fundamental frequency whose period is about 18 to 20 m.s. However, the experimental data has a second harmonic of about 2.5 m.s. period which is not seen in the model data.

#### Run 5

Run 5 simulated two, 18 m.s. nominal pulses. Nominal off time between pulses was 20 m.s. Engine attitude was up-firing. Other data was as that of preceeding runs.

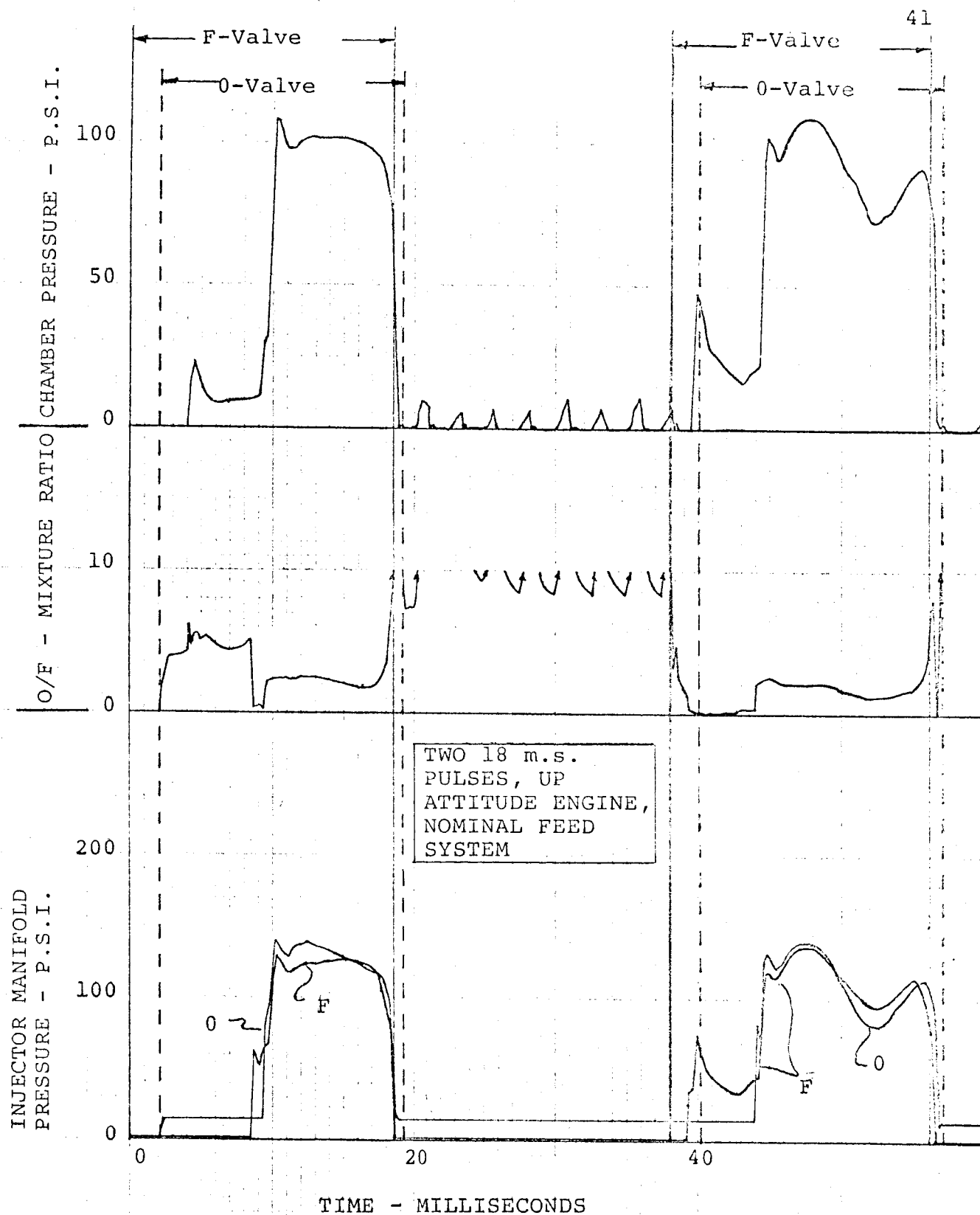
Chamber pressure, mixture ratio, and injector manifold dribble volume pressure are shown in Figure 16. The second pulse differs from the first due to incomplete dribble volume emptying during the short off time. There are similar distinctions exhibited in test data.

Figure 17 shows the total mass of each propellant remaining in their dribble volumes during the run. It also shows the variation in combustion time delay,  $\tau$ .

#### Runs 6 and 7

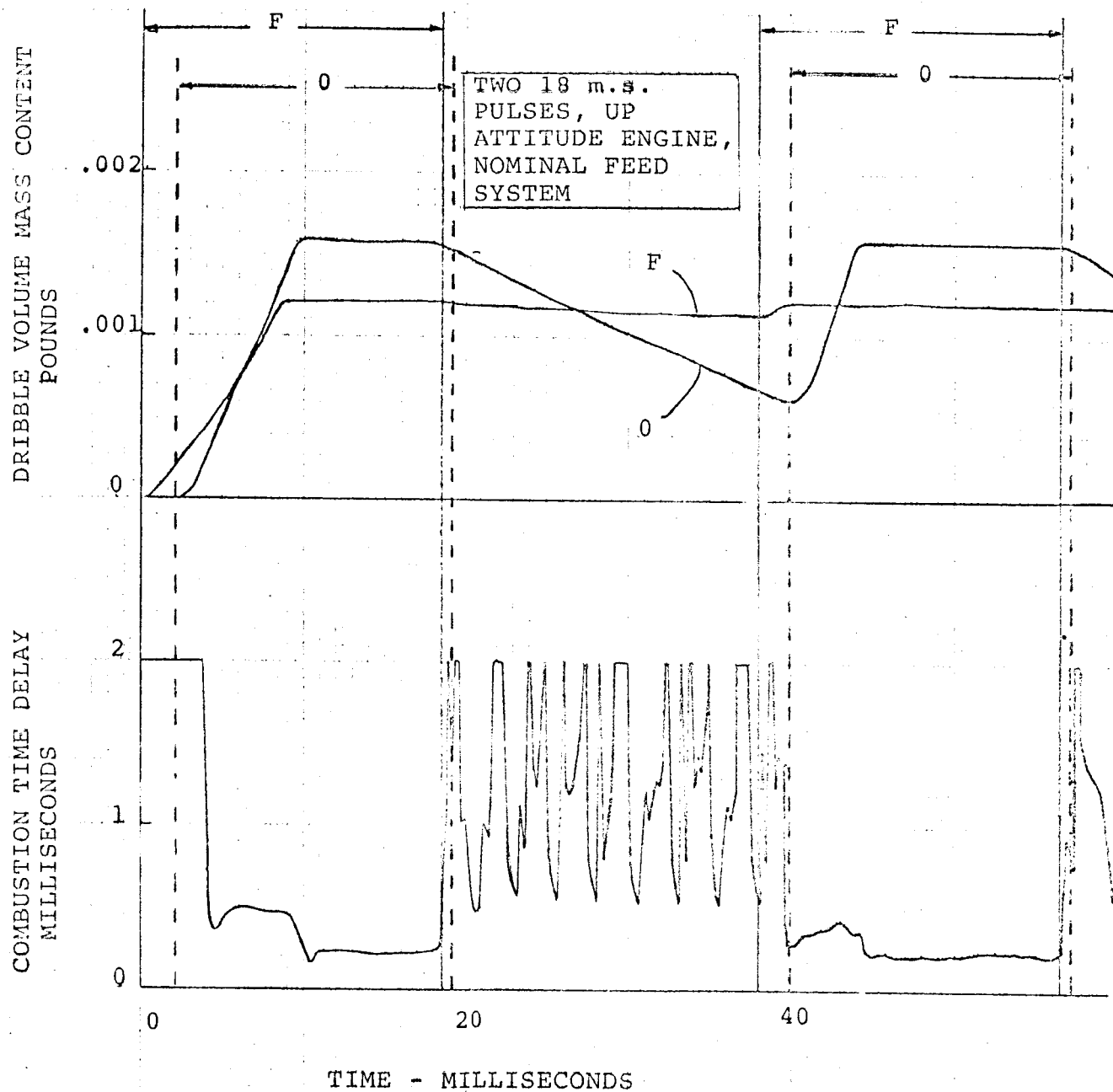
These two runs each had two, twelve m.s. pulses with twelve m.s. off time between pulses. However, during both valve opening and valve closure, the oxidizer valve led the fuel valve by two m.s. Run 6 represents an up-firing engine while run 7 is for a down-firing engine.

Three pages of graphs, Figures 18, 19 and 20, are shown for run 6. Only the standard chamber pressure, mixture ratio, and injector manifold pressure graphs are presented for run 7



RUN - 5

Figure 16.



RUN - 5

Figure 17

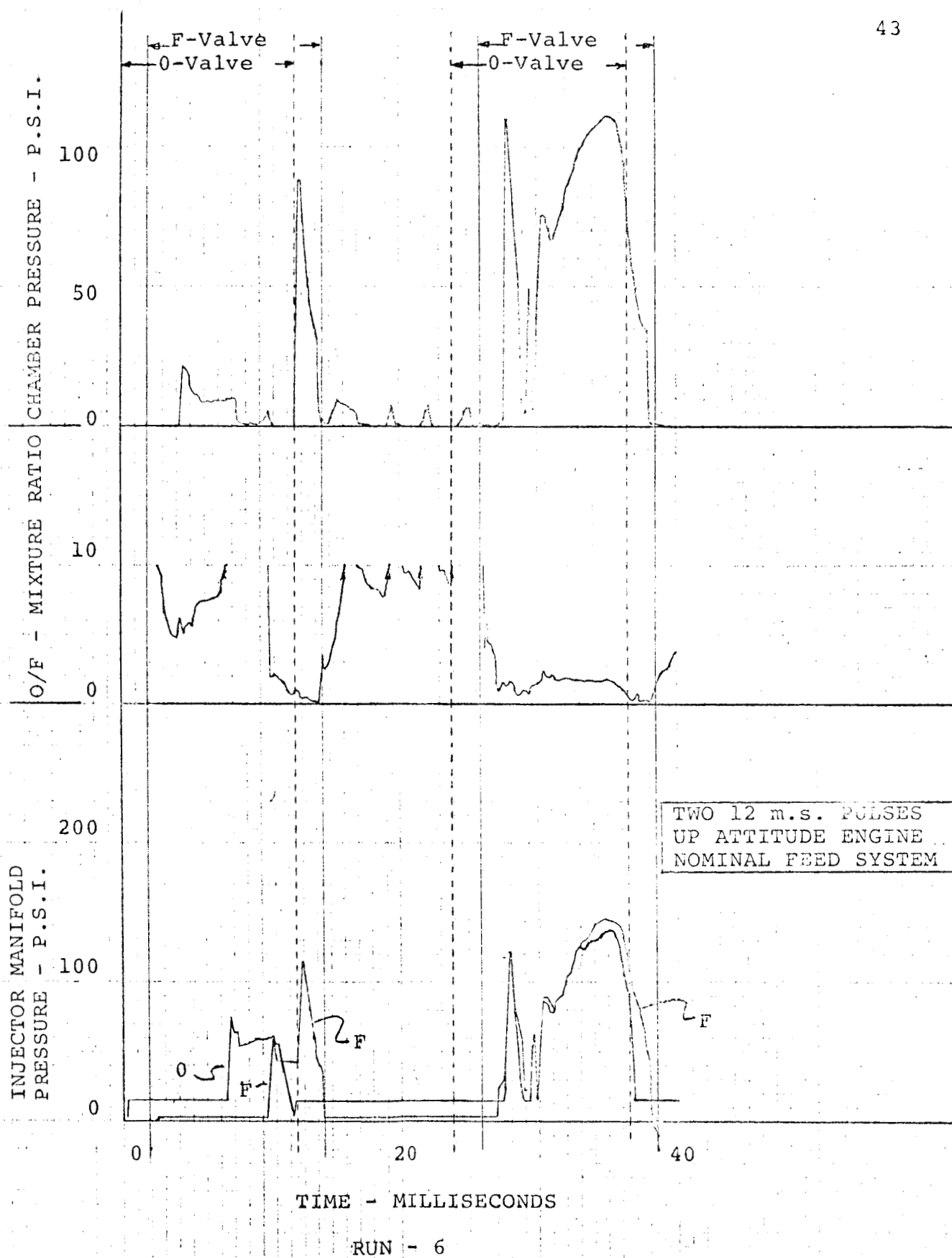
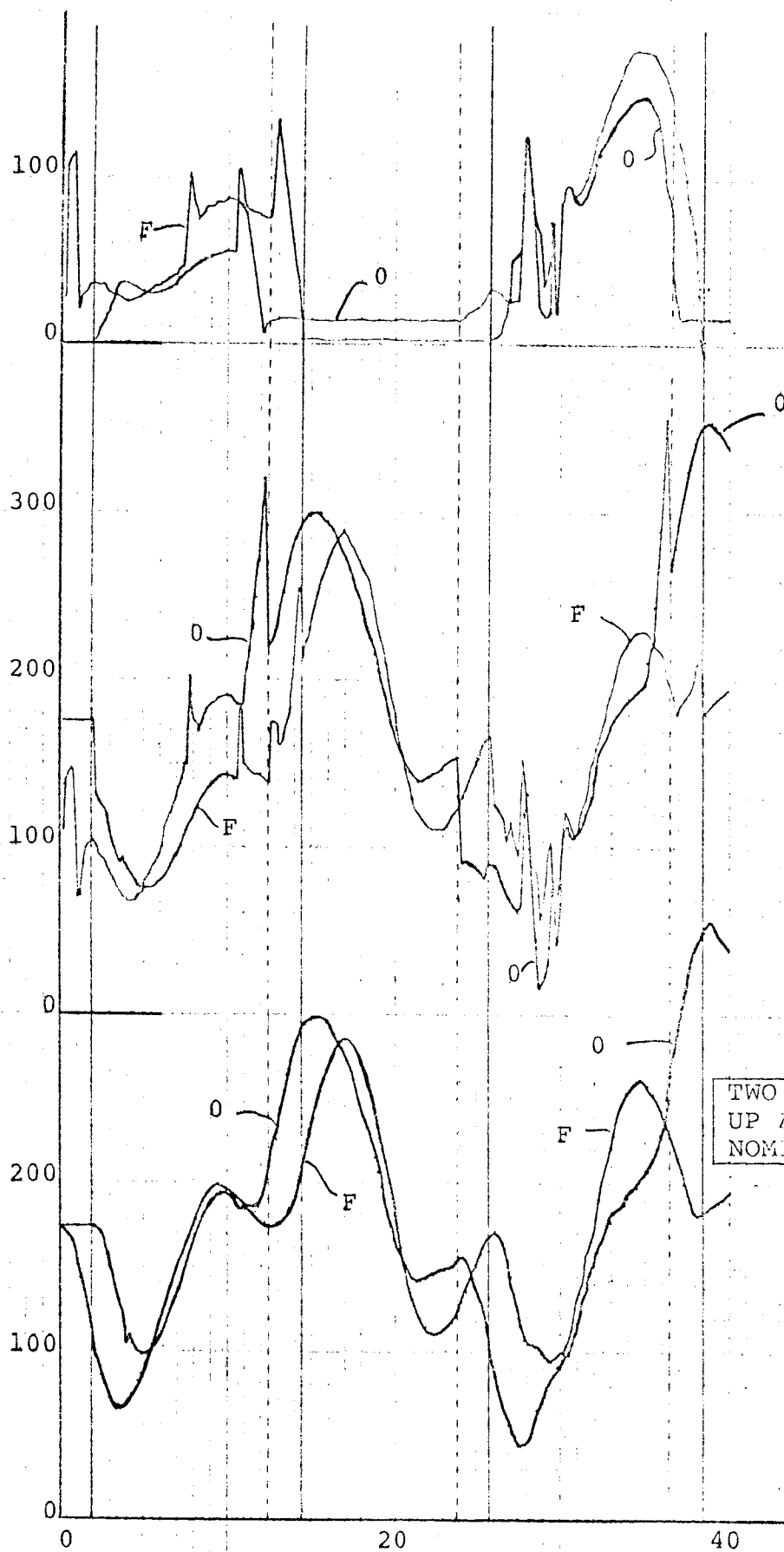


Figure 18

PREIGNITER INJECTOR  
PRESSURE - P.S.I.

UPSTREAM VALVE PRESSURE - P.S.I.

Y-BLOCK PRESSURE - PSI

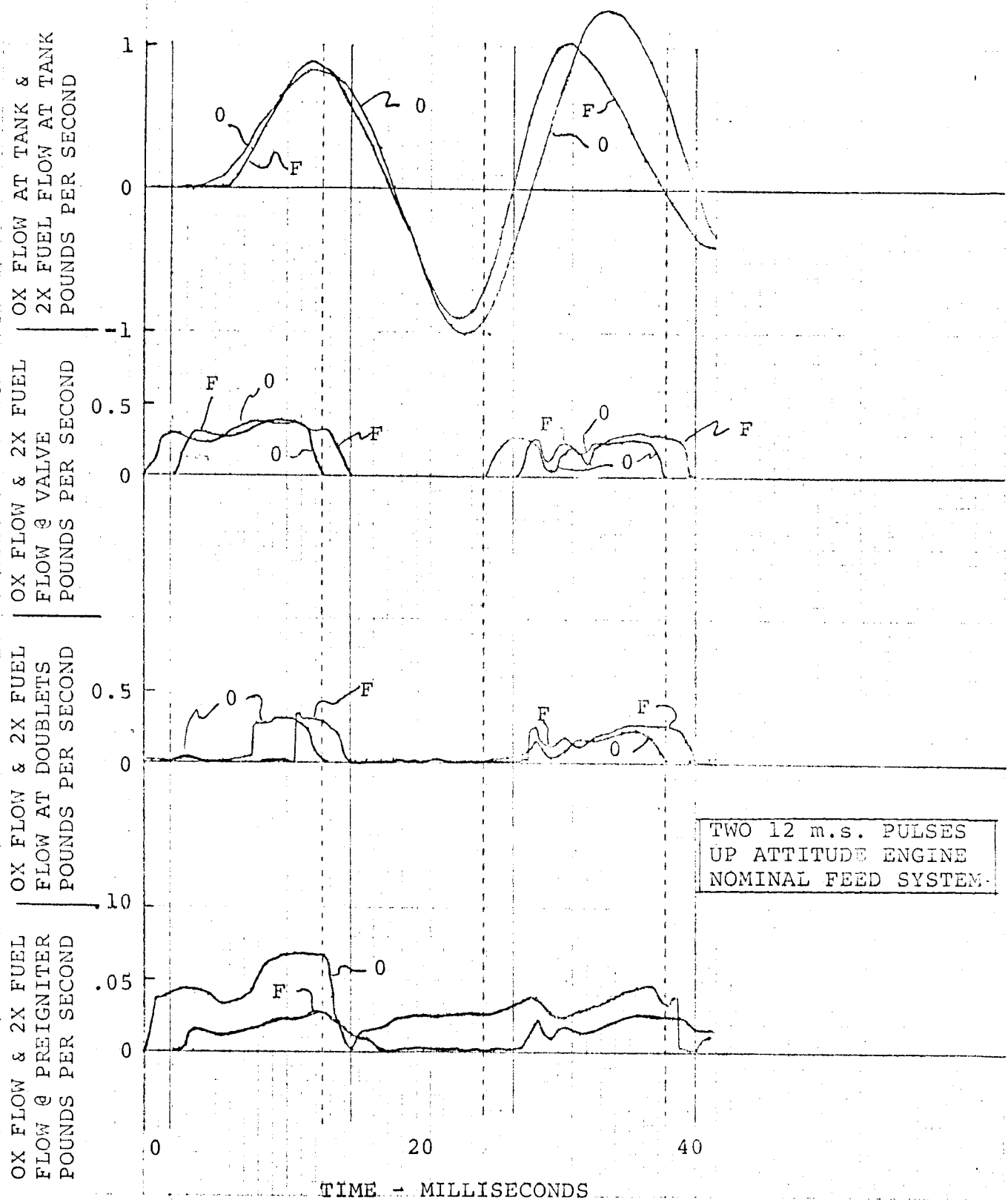


TIME - MILLISECONDS

RUN - 6

Figure 19





RUN - 6

Figure 20

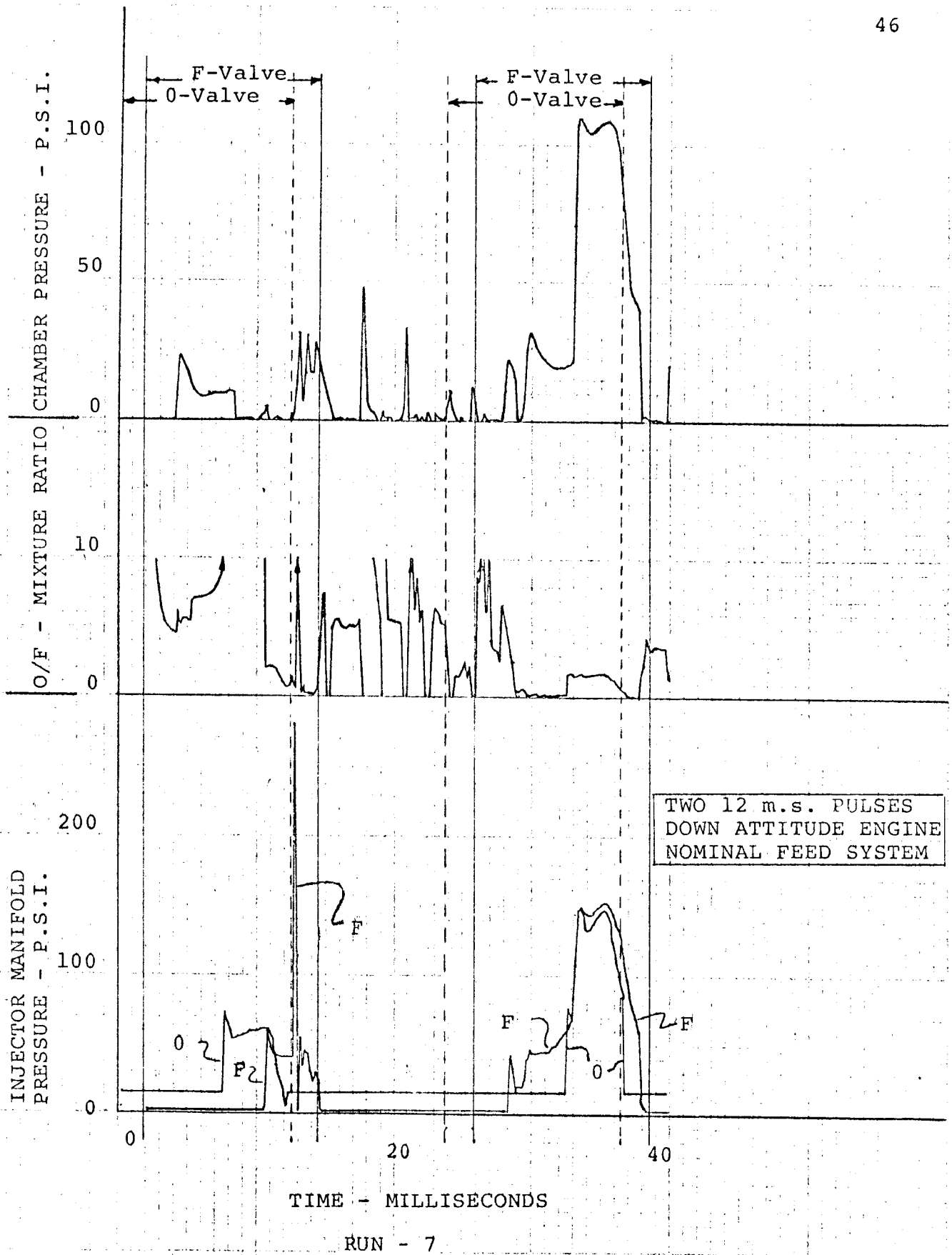


Figure 21

in Figure 21. Note that with oxidizer leads the fuel dribble volume fills just prior to valve closure for a twelve m.s. pulse. This inhibits chamber ignition.

Oscillations in the feed line pressures appear to have primary frequencies of 56 Hertz in the fuel and 50 Hertz in the oxidizer feed line. These are approximately twice as large as indicated by test data. In addition, the near discontinuities in the upstream valve pressure coincident with valve closures are more indicative of the computational instability tendencies than of any physically reasonable system activity.

#### Run 12

In this run, the capacitance representing the feed lines for the three clusters of non-firing engines was reduced by 75 percent. The engines were up-firing with two, twelve m.s. pulses and 10 m.s. off time. The fuel valve opened leading the oxidizer valve by 2 m.s. The fuel valve lead during closure was 0.7 m.s.

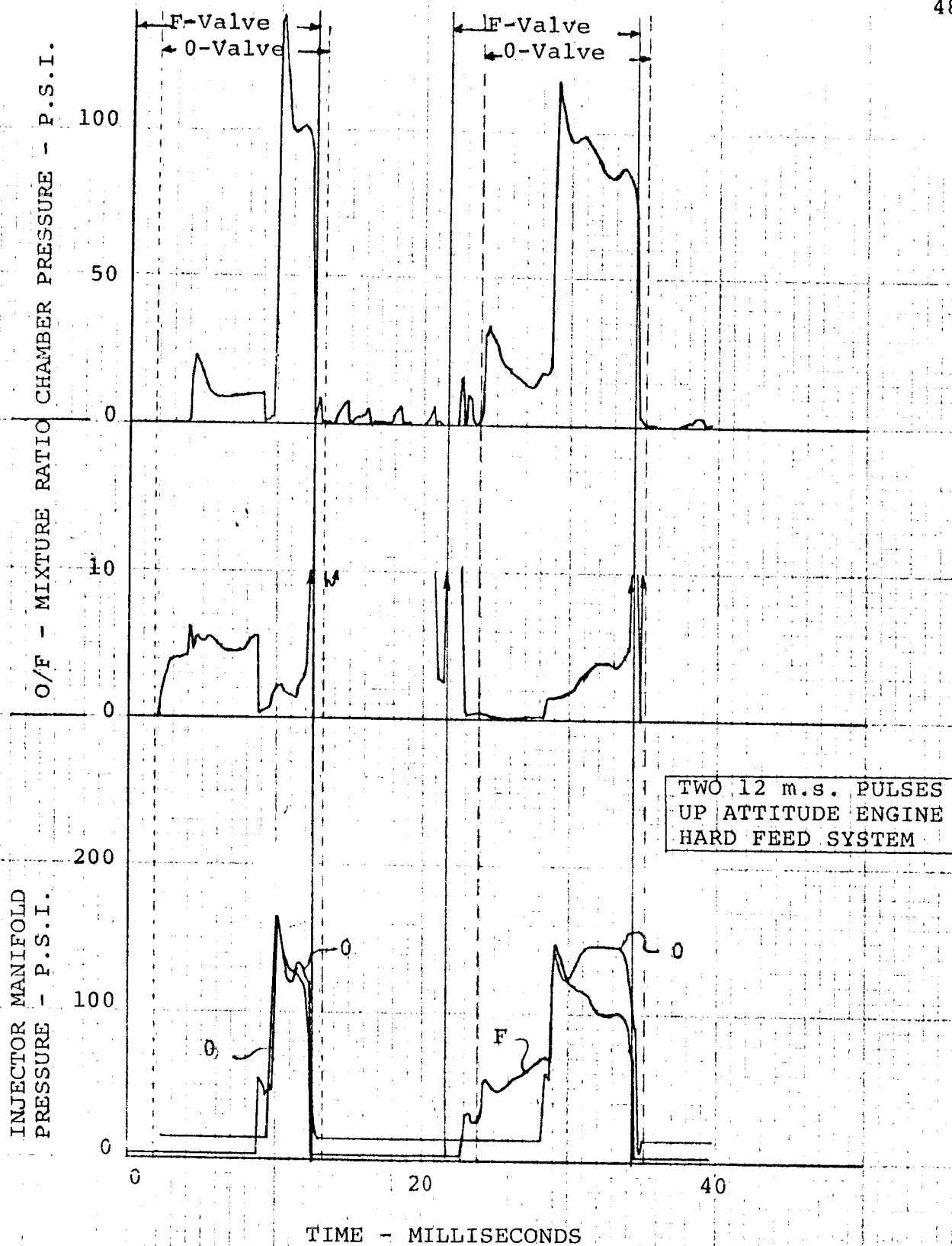
Figure 22 shows that the levels of chamber pressure attained with the harder feed system were more intense.

Figure 23 shows that the pressure excursions in the feed lines were significantly more intense and of a slightly higher frequency than for the nominal system.

A slight reduction in amplitude of tank flow oscillations but an increase in frequency is shown in Figure 24.

#### Run 14

The engine operating conditions in this run are the same as those in run 12. In this case, the nominal feed system is



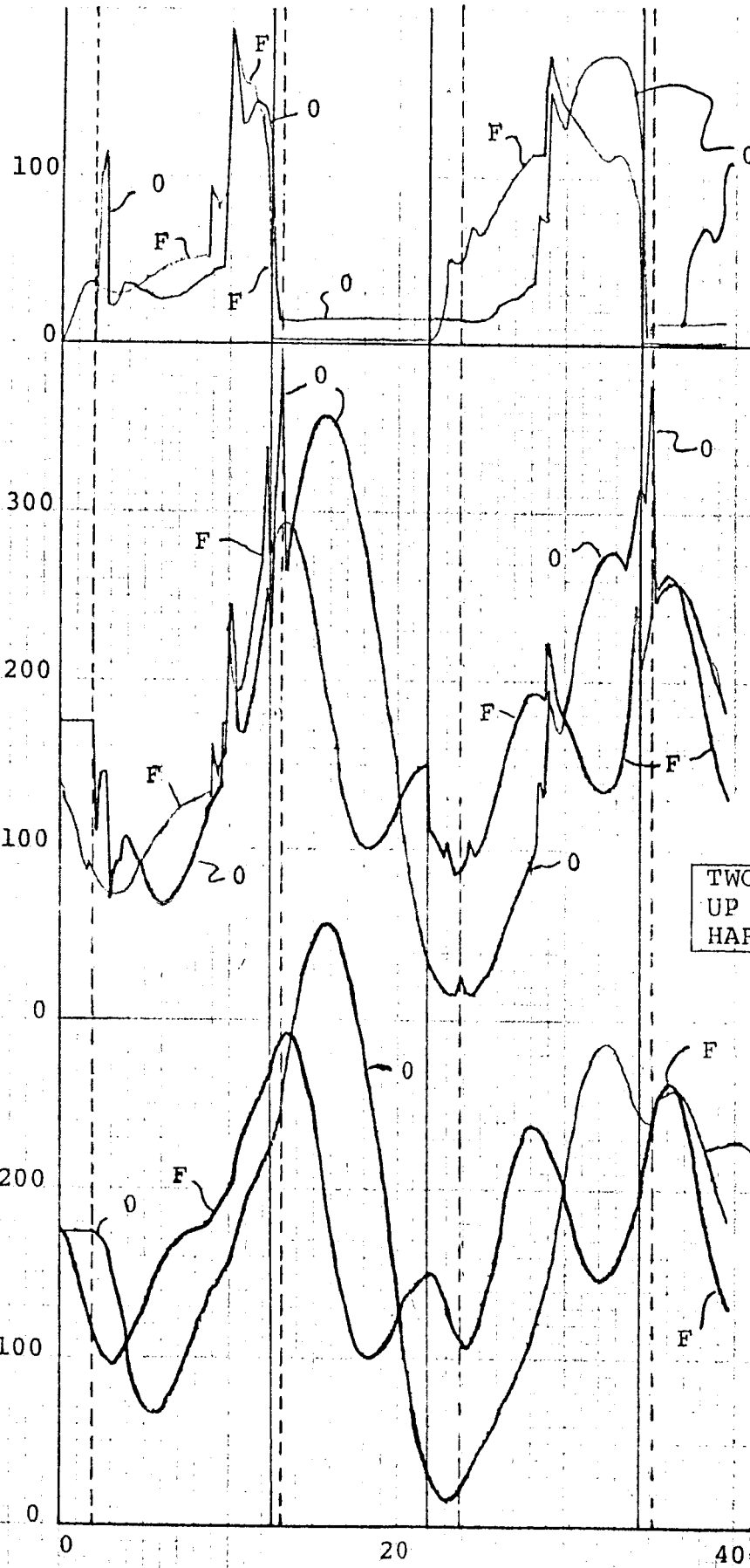
RUN - 12

Figure 22

PREIGNITER INJECTOR  
PRESSURE - P.S.I.

UPSTREAM VALVE PRESSURE - P.S.I.

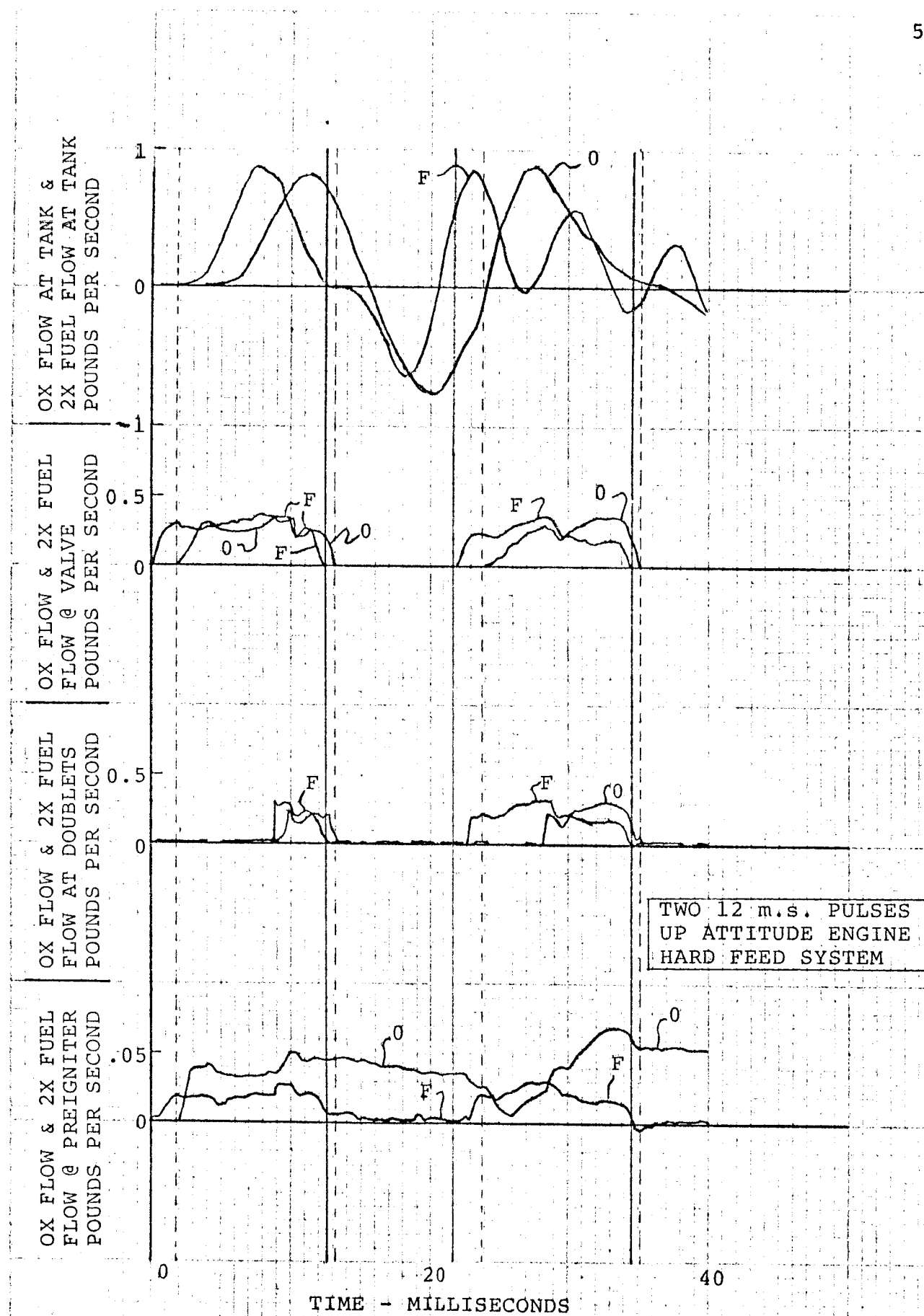
Y-BLOCK PRESSURE - PSI



TIME - MILLISECONDS

RUN - 12

Figure 23



TIME - MILLISECONDS

RUN - 12

Figure 24

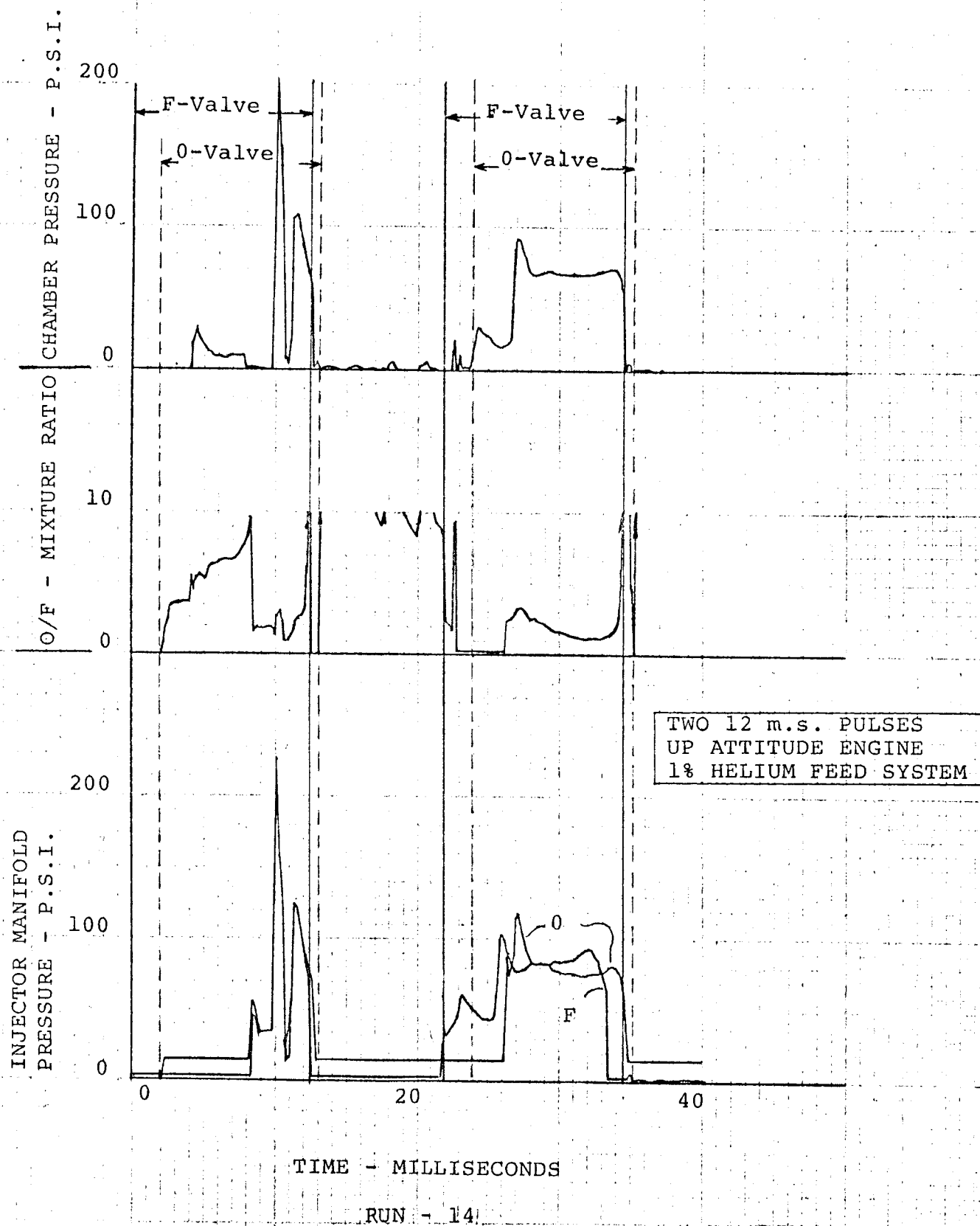
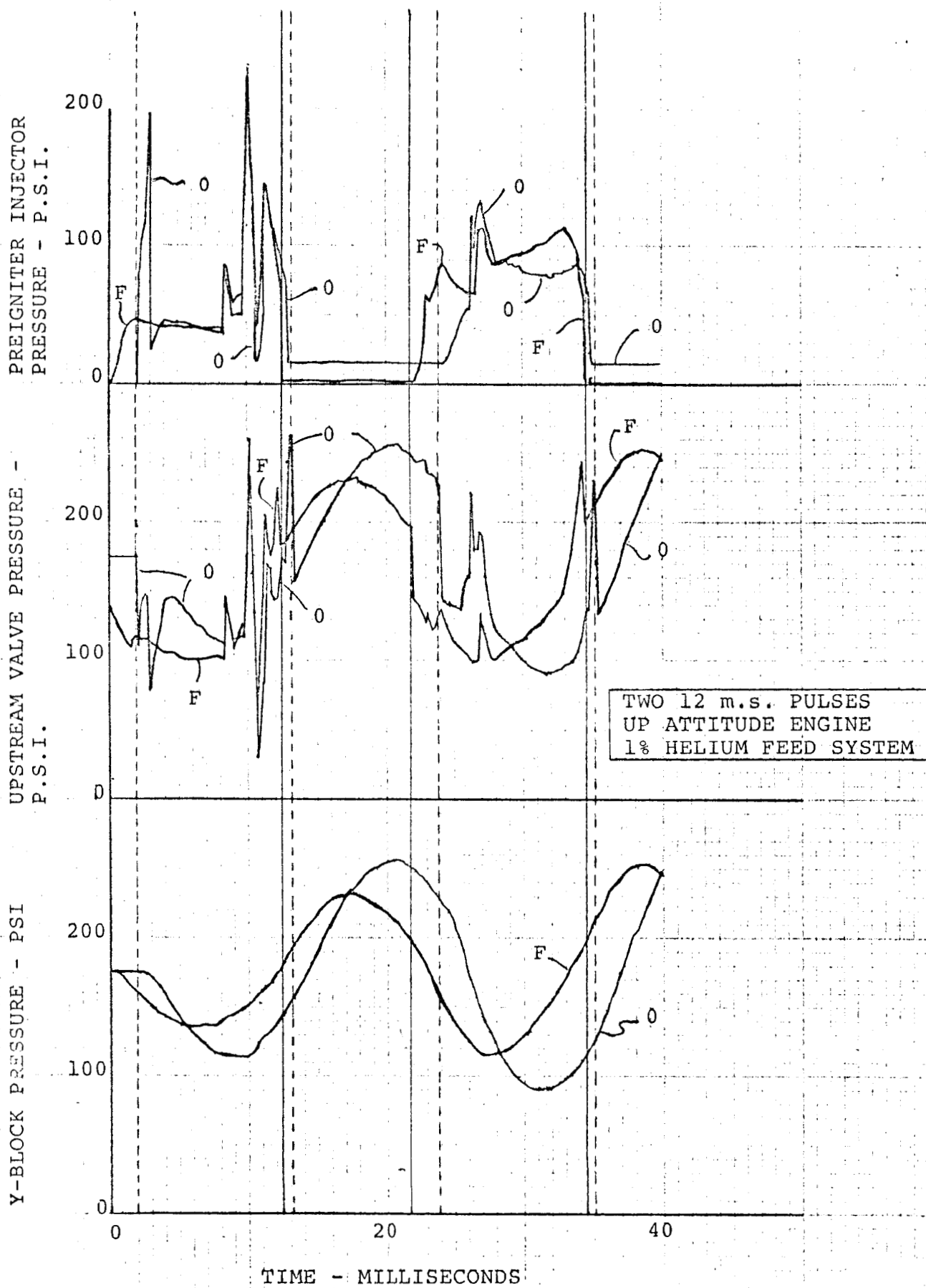


Figure 25



RUN - 14

Figure 26



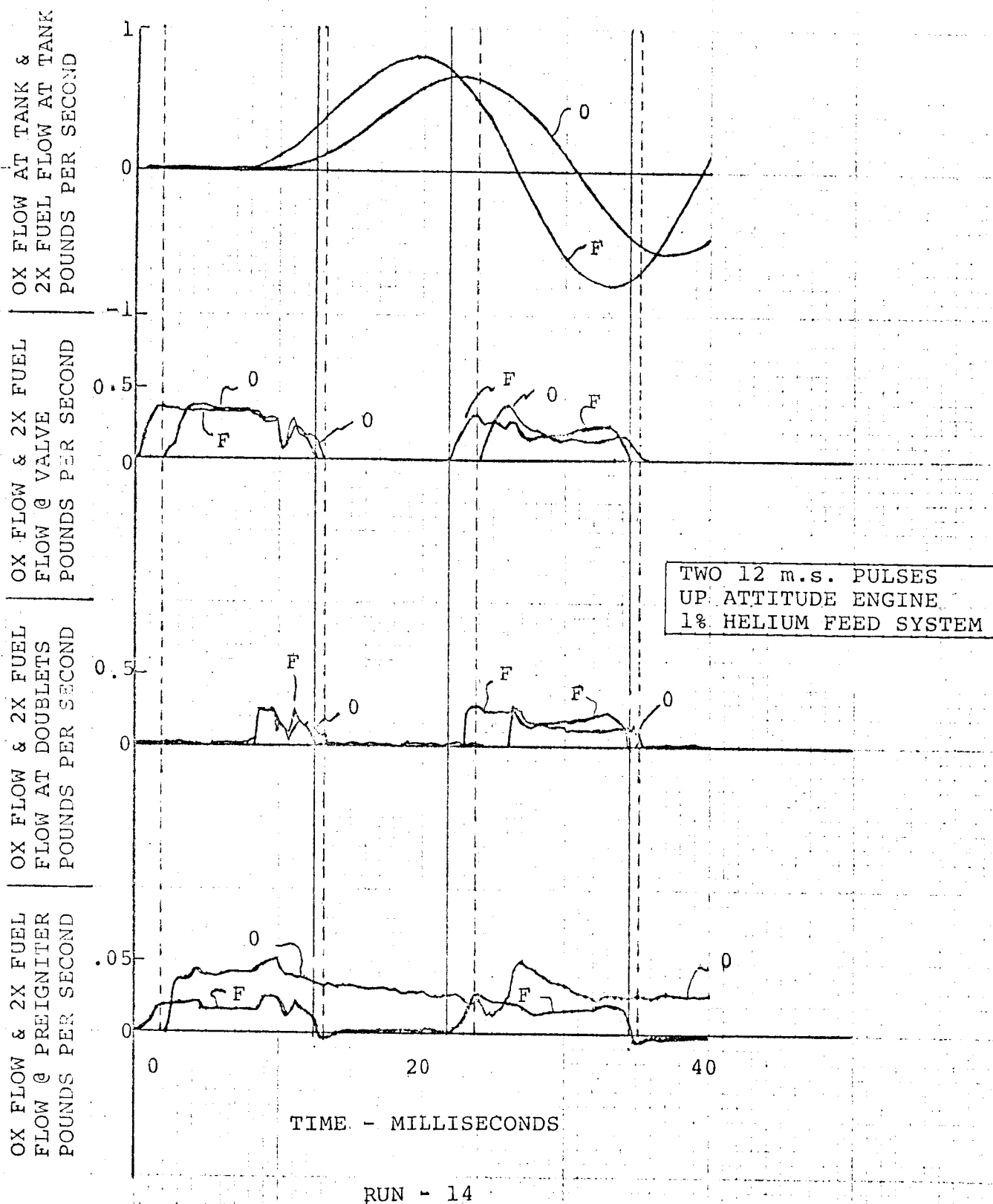


Figure 27

used but the propellants in the feed line are presumed to contain entrained helium in the amount of 1 percent by volume at 70°F and 175 psia.

Engine performance is very rough during the first pulse. . Note that a larger scale had to be used for chamber pressure in Figure 26. On the other hand, the feed line excursions were very smooth as can be observed from Y-block pressures in Figure 26. This is due to the accumulator effect of the entrained helium. Line frequencies are somewhat reduced in this run, but they are still higher than experimental values; i.e., 26 Hertz for fuel and 20 Hertz for oxidizer.

Figure 27 shows much smoother flow rates in the feed lines due to the entrained helium.

## CONCLUSIONS

The number of lumped feed line elements utilized in the digital program for this study was insufficient for high precision. Nevertheless, reasonable amplitudes were realized except during extreme transients. Some frequencies could have been off by a factor as high as two.

The combustor model, relying upon mixture ratio only for characteristic velocity, performed well at high pressure but was incapable of representing the chamber pressure when operating conditions were greatly different from steady state design conditions. Careful evaluation of the results indicated that the typical experimental chamber pressure decay is characteristic of the emptying-tank effect of the chamber volume. No allowance for this was in the combustor model.

Large backflow tendencies from the combustion chamber to injector were detected following preigniter ignition and during tail-off. Such flow and its apparently significant effects on injector pressurization, main chamber ignition, and chamber pressure build-up were not anticipated or properly taken into account in either the injector model or the combustor model. However, their significant role was identified in this study.

The attempted simulation produced results in such detail that it provided insight into the engine's complex operation and permitted considerable evaluation of the model. Comparisons with experimental measurements suggested physical mechanisms potentially responsible for discrepancies between the model and the hardware.

The results indicate that the models are not yet ready for precision simulation utilization. This analytic procedure, however, may be used to indicate qualitative changes in propulsion parameters caused by hardware changes or anomalies.

## RECOMMENDATIONS

It is considered that the general qualities of the simulation are valid. Several details are inadequate for desired precision. The behavior of the various models was too complex for analog computations, and it readily indicated weak points once digital computations were employed. However, on a digital computer model alterations were not as convenient as on an analog machine for which many of the models had been designed. As an alternative to employing clumsy model alterations, a model simplifying computer logic was utilized. Nevertheless, the results did show that gas injected propellants (or distributed accumulators) reduces the severity of feed line oscillations.

To more effectively utilize the advantages of digital machines, it is recommended that the entire simulation be expanded and detailed as a second phase of the study in which systematic improvements are made based on the knowledge and results gained in this study. Suggested modifications for each type of model will be given.

Feed Lines

If a sufficiently large number of lumped feed-line elements are used, they will give good performance. However, lumping involves the discretization of the spatial variation of the flow properties. Numericalizing the resulting ordinary differential equations for digital computers makes time a discrete variable. Difficulty arises if the discrete units of space

and time are not properly related. Digital methods are now available for treating this problem by the method of characteristics with non-linear friction included (Reference 3). Furthermore, the method makes the need for explicitly lumping parameters unnecessary. The acquisition and utilization of a good, versatile program for method of characteristic solutions is recommended for the feed lines.

### Injectors

The development of a general flow model based on a dribble volume considered as a tank is recommended. The tank should be capable of containing not only reactable material in both liquid and vapor phases, as in the present model, but also inert material in the gaseous phase to allow for combustion product backflow.

The resistive elements separating the dribble volume from the remainder of the injector should be capable of flow in any direction of any type of fluid. In addition, the flow through the preigniter and that through the main orifices should not meet prior to reaction. They should be coupled through a distinct preigniter combustor discharging into the main chamber.

Specifically, it is recommended that various multi-phase tank-orifice models be studied on a digital computer until flows of the types seen to be necessary in this study are attained.

### Combustor

It is recommended that two distinct combustion chambers be employed, one for the preigniter and one for the main chamber.

The characteristic velocity should be dependent not only

upon mixture ratio but also upon chamber pressure. This should be done so that the pressure in the chamber cannot drop faster than the chamber can empty its contents to a vacuum through a choked nozzle.

The time delay mechanism should also be strengthened so that it is compatible with the remainder of the reaction model. A zero pressure ignition delay in the chamber (as employed in the present General Electric model) is unreasonable. The ignition delay is that at the chamber pressure prevailing when ignition occurs. The pre-pressurization is due to vapor in-flow from the injector, choked out-flow through the nozzle, and ultimately preigniter combustion exhaust as far as the main chamber is concerned.

## APPENDIX A

Fundamentals of Lumped Parameter Equations

The formulation of the flow in a propellant system requires a consideration of fluid dynamics, thermodynamics, and the geometrical and mechanical characteristics of the propellant feed-system structure. Since the flow variables are functions of both time and spatial coordinates, the formulation that follows is developed from simplified fluid kinetic and thermodynamic theory and the system structure is treated as straight thin-walled piping.

The five basic equations utilized follow.

Flow Geometry:

$$(1) \quad \dot{W} = \int_A \vec{G} \cdot d\vec{S}$$

where  $\vec{G} \equiv \rho \vec{V}$ ,

Continuity:

$$(2) \quad \frac{d}{dt} \int_V \rho dv + \int_S \vec{G} \cdot d\vec{S} = 0$$

Momentum:

$$(3) \quad \sum \vec{F} = \frac{d}{dt} \int_V \vec{G} dv + \int_S \vec{V} (\vec{G} \cdot d\vec{S})$$

where  $v$  is the control volume and  $S$  is its surface area.

Thermodynamic state:

$$\rho = \rho(P)$$

i.e., a barotropic relationship is presumed to exist. It is described by the bulk modulus for the appropriate process



$$(4) \quad B = \rho \frac{dP}{d\rho}$$

Piping Structure:

$$(5) \quad \frac{dA}{dt} = \frac{A}{E(D_o/D_i - 1)} \frac{dP}{dt}$$

The simplification of the above system of equations results by judiciously lumping parameters, i.e., using spatially averaged values of certain properties in various equations. This procedure is justified for small spatial regions and thus requires a large number of such regions to represent an entire flow system.

Letting  $\bar{\rho}$  be the average density over a small one-dimensional control volume,  $v$ , of length  $\Delta l$  and time-dependent, spatially-averaged, cross-sectional area  $\bar{A}$ , equation (2) reduces to

$$(6) \quad \frac{d}{dt} (\rho v) = v \frac{d\bar{\rho}}{dt} + \bar{\rho} \frac{dv}{dt} = - \int_S \vec{G} \cdot d\vec{S}$$

But from equation (5)

$$(7) \quad \frac{dv}{dt} = \frac{dv}{d\bar{A}} \frac{d\bar{A}}{dt} = \Delta l \frac{d\bar{A}}{dt} = \frac{v}{E(D_o/D_i - 1)} \frac{d\bar{P}}{dt}$$

By utilizing equation (4)

$$(8) \quad \frac{d\bar{\rho}}{dt} = \frac{d\bar{\rho}}{d\bar{P}} \frac{d\bar{P}}{dt} = \frac{\bar{\rho}}{B} \frac{d\bar{P}}{dt}$$

Also, equation (1) results in

$$(9) \quad \int_S \vec{G} \cdot d\vec{S} = \int_{A_b} \vec{G} \cdot d\vec{S} - \int_{A_a} \vec{G} \cdot d\vec{S} = \dot{W}_b - \dot{W}_a$$

where the subscripts a and b refer to the cross-sectional surfaces through which fluid enters and leaves  $v$  respectively.

Substituting (7), (8) and (9) into (6) yields

$$(10) \quad \frac{v\bar{\rho}}{B} \frac{d\bar{P}}{dt} + \frac{v\bar{\rho}}{E(D_o/D_i-1)} \frac{d\bar{P}}{dt} = - (\dot{W}_b - \dot{W}_a)$$

or

$$(11) \quad \frac{v\bar{\rho}}{B_e} \frac{d\bar{P}}{dt} = \frac{v}{a^2} \frac{d\bar{P}}{dt} = \dot{W}_a - \dot{W}_b$$

where the equivalent bulk modulus,  $B_e$  is

$$(12) \quad 1/B_e = 1/B + 1/E(D_o/D_i-1)$$

and the velocity of propagation,  $a$ , of a small pressure disturbance in the fluid medium of modulus  $B$  contained in an elastic pipe of modulus  $E$  with inner and outer diameter  $D_i$  and  $D_o$  respectively can easily be shown to be

$$(13) \quad a = \sqrt{B_e/\rho}$$

A final form for (11) is

$$(14) \quad \dot{W}_a - \dot{W}_b = C \frac{dP}{dt}$$

which is equivalent to a lumped capacitive element of an electrical circuit.  $P$  represents the instantaneous pressure most representative of the lumped region and  $C$  is the capacitance of the region.  $C = \frac{v}{a^2}$  in a simple elastic pipe

or in a more complicated situation can be phenomenologically defined by equation (14) so as to insure the mass continuity for all fluid states in a conduit of some characteristic structural integrity and geometry.

Equation (14) has utilized all of the basic equations of the system except the momentum equation, (3). For one-dimensional flow, the momentum equation in the direction of flow simplifies to

$$(15) \quad \sum F = \frac{d}{dt}(\bar{\rho}\bar{A}\Delta_1\bar{V}) + \rho_b A_b V_b^2 - \rho_a A_a V_a^2$$

The resultant external force on the small region is presumed to be due to surface forces only. These are:

$$\text{Pressure force on upstream end} = P_a A_a$$

$$\text{pressure force on downstream end} = -P_b A_b$$

$$\text{pressure force on lateral surface} = \int_{S_1} P \sin \alpha \, dS \approx \bar{P} \sin \alpha \, \Delta S_1$$

$$\text{friction force on lateral surface} = \int_{S_1} \tau_s \cos \alpha \, dS \approx \bar{\tau}_s \cos \alpha \, \Delta S_1$$

where  $\alpha$  is the angle of divergence of a small region of the fluid conduit and  $\tau_s$  is the shear stress at the lateral surface  $\Delta S_1$ . Thus

$$(16) \quad \sum F = P_a A_a - P_b A_b + \bar{P} \sin \alpha \, \Delta S_1 - \bar{\tau}_s \cos \alpha \, \Delta S_1$$

Substituting (16) into (15) and using the delta operator

$\Delta Q \equiv Q_b - Q_a$  we arrive at

$$(17) \quad -\Delta(PA) + \bar{P} \sin \alpha \, \Delta S_1 - \bar{\tau} \cos \alpha \, \Delta S_1 = \frac{d}{dt}(\bar{\rho}\bar{A}\Delta_1\bar{V}) + \Delta(\rho AV^2)$$

$$= \Delta_1 \frac{d\bar{W}}{dt} + \Delta(\rho AV^2)$$

or rearranging

$$(18) \quad -\Delta P = \frac{\Delta_1}{\bar{A}} \frac{d\dot{W}}{dt} + \frac{\bar{V}\Delta_1}{\bar{A}} \Delta\dot{W} + \frac{\bar{W}}{\bar{A}} \Delta V \Delta_1 + \frac{\bar{P}}{\bar{A}} (\Delta A - \sin \alpha \Delta S_1) \Delta_1 \\ + \frac{\bar{\tau}_s}{\bar{A}} \cos \alpha \Delta S_1 \Delta_1$$

For low velocity flow, the second term on the right side of (18) may be neglected without introducing significant error. The resulting equation represents the spatial pressure change as a quantity dependent upon two types of functions, a spatial function and a rate function.

The spatial function

$$(19) \quad -\Delta P_s = \frac{\bar{W}}{\bar{A}} \Delta V \Delta_1 + \frac{\bar{P}}{\bar{A}} (\Delta A - \sin \alpha \Delta S_1) \Delta_1 + \frac{\bar{\tau}_s}{\bar{A}} \cos \alpha \Delta S_1 \Delta_1$$

depends upon friction, flow geometry, and the fluid state. It exists during steady flow and is identical to steady-flow pressure variations. In steady state fluid mechanics it is customarily represented in the form of a flow resistance as

$$(20) \quad -\Delta P_s = R \dot{W}$$

where, in a simple case,

$$R = f \frac{16}{D_i} \frac{1}{2\rho A^2}$$

The rate function

$$(21) \quad -\Delta P_t = \frac{\Delta_1}{\bar{A}} \frac{d\dot{W}}{dt}$$

is purely a transient phenomena. It may be represented as a lumped inductive element in the form

$$(22) \quad -\Delta P_t = L \frac{d\dot{W}}{dt}$$

where  $L = \int \frac{d_1}{A}$

Thus the requirements of the momentum equation are completely satisfied by equations (18), (19), and (21)

$$(23) \quad \Delta P = \Delta P_s + \Delta P_t$$

Substituting from (20) and (22) yields

$$(24) \quad P_a - P_b = R\dot{W}|\dot{W}| + L \frac{d\dot{W}}{dt}$$

where  $\dot{W}$  represents the mass flow rate most representative of that in the lumped region,  $R$  is the steady state frictional resistance and/or flow coefficient, and  $L$  is the equivalent inductance  $L = \int \frac{dl}{A}$

One may consider a flow passage as a distribution of non-interacting capacitive, inductive, and resistive elements each partially satisfying the system of equations (14) and (24). Insofar as spatially averaged variables are utilized in the equations, it is seen that this process is one of lumping a distributed phenomena into a finite number of single elements. Thus, the use of a larger number of elements produces a better representation of a flow system.

## APPENDIX B

Linearized Combustion Delay

The equation for the effective time delay,  $\tau$ , between propellant injection into the chamber and the generation of combustion product gas, based on vaporization controlled reaction of hypergolic propellants, is (Reference 2)

$$\frac{d\tau(t)}{dt} = 1 - \frac{q(t)}{q(t-\tau)}$$

The rate function,  $q$ , depends upon chamber pressure (Reference 6). In this study,  $q$  is normalized with respect to its value for zero pressure ignition, i.e., for  $P = 0$ ,  $q = 1$  and  $\tau = \tau_0$  (Reference 2).

An approximate solution of the above differential equation is obtained by expanding  $\tau$  in a Taylor's series.

$$\tau(t-\tau) = \tau(t) + \frac{d\tau(t)}{dt}(-\tau) + \frac{d^2\tau(t)}{dt^2} \frac{(-\tau)^2}{2} + \dots$$

Neglecting second and higher order terms gives

$$\frac{d\tau(t)}{dt} \approx \frac{\tau(t) - \tau(t-\tau)}{\tau} = 1 - \frac{\tau(t-\tau)}{\tau(t)}$$

Substituting this in the first above relation yields

$$\tau(t-\tau)q(t-\tau) = \tau(t)q(t) = \text{const} \equiv \tau_0$$

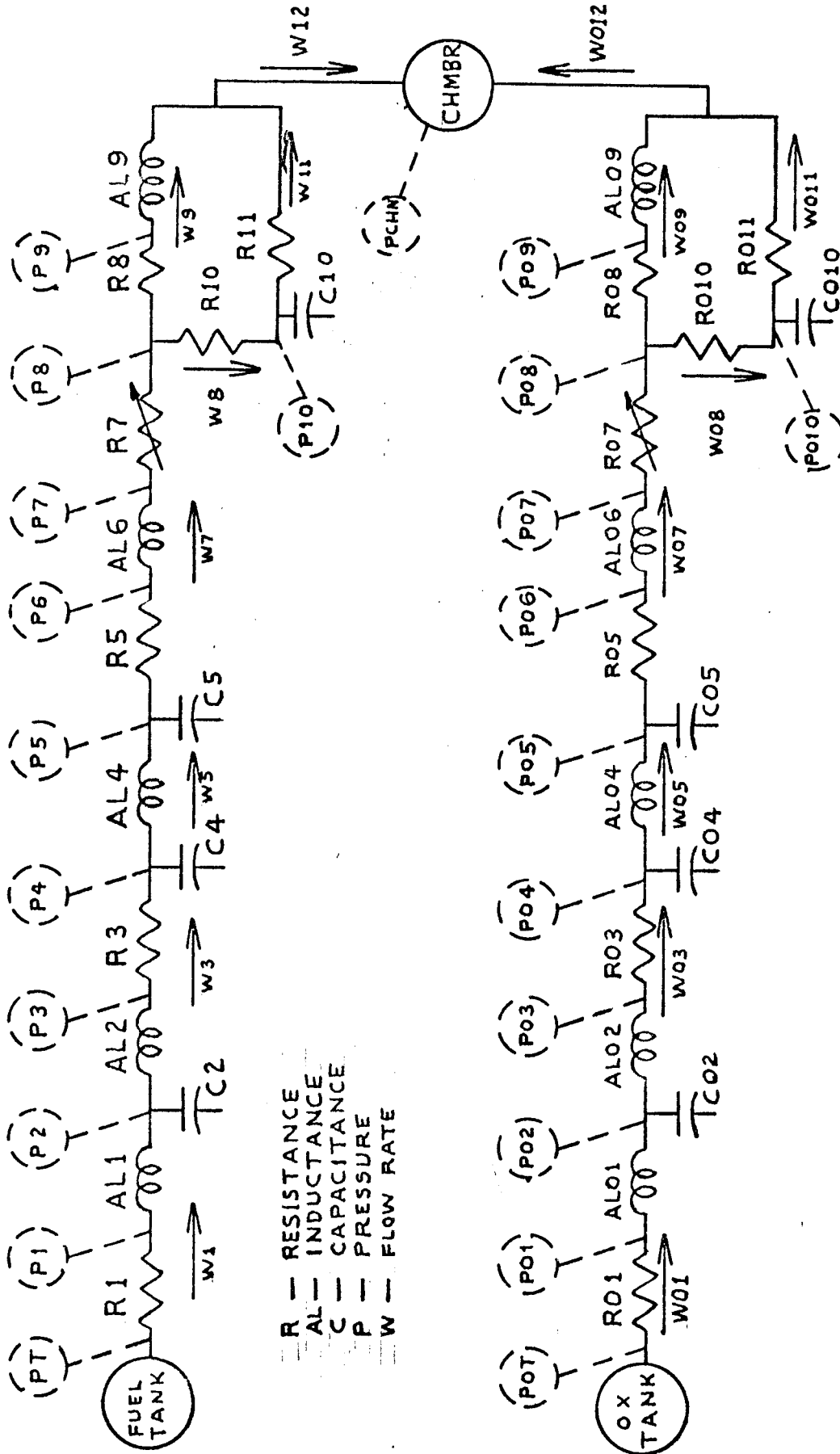
## APPENDIX C

Computer Nomenclature and Model Constants

The nomenclature used in the computer program for pressures, flows, and element parameters is shown in Figure 28. Note that the letter "O" distinguishes between an oxidizer system quantity and the same quantity for the fuel system.

Line properties for nominal runs are in table C-1. Values which were changed for special runs are shown in table C-2.

Propellant properties, injector parameters, and combustor constants are given in table C-3.



COMPUTER PROGRAM NOMENCLATURE

FIGURE 28



TABLE C-1

L/M-RCS FEED SYSTEM PARAMETERS BASED ON ENGINE #13

(NOMINAL)

FUEL

R1	3.57
R3	10.37
R5	1386
R8	389000

OXIDIZERRESISTANCE -  $(\text{LBF} \cdot \text{SEC}^2) / (\text{IN}^2 \cdot \text{LBM}^2)$ 

R01	1.99
R03	5.92
R05	40.815
R08	17600

CAPACITANCE -  $(\text{LBM} \cdot \text{IN}^2) / \text{LBF}$ 

C2	$26.86 \times 10^{-6}$
C4	$2.824 \times 10^{-6}$
C5	$2.824 \times 10^{-6}$

C02	$49.905 \times 10^{-6}$
C04	$4.78 \times 10^{-6}$
C05	$4.78 \times 10^{-6}$

INDUCTANCE -  $(\text{LBF} \cdot \text{SEC}^2) / (\text{LBM} \cdot \text{IN}^2)$ 

AL1	.2110
AL2	.2110
AL4	.7221
AL6	.28031
AL9	1.83

AL01	.1641
AL02	.1641
AL04	.6565
AL06	.28031
AL09	1.32

TANK PRESSURE -  $\text{LBF} / \text{IN}^2$ 

PT	175
----	-----

POT	175
-----	-----

TABLE C-2  
L/M-RCS FEED SYSTEM PARAMETERS  
(SUBSTITUTED VALUES FOR SPECIAL RUNS)

## RUN 12

C2	$9.077 \times 10^{-6}$
----	------------------------

C02	$15.878 \times 10^{-6}$
-----	-------------------------

## RUN 14

C2	$145.0 \times 10^{-6}$
C4	$15.25 \times 10^{-6}$
C5	$15.25 \times 10^{-6}$

C02	$235.5 \times 10^{-6}$
C04	$22.55 \times 10^{-6}$
C05	$22.55 \times 10^{-6}$

TABLE C-3  
L/M-RCS ENGINE PARAMETERS  
AND PROPERTIES FOR SIMULATION

	FUEL	OX
INJECTOR $R_1 - (\text{LBF-SEC}^2)/(\text{IN}^2\text{-LBM}^2)$	1229.0	4.0149
INJECTOR $L_1 - (\text{LBF-SEC}^2)/(\text{LBM-IN}^2)$	0.28031	0.28031
LIQUID $R_a - (\text{LBF-SEC}^2)/(\text{IN}^2\text{-LBM}^2)$	1650.0	284.0
LIQUID $R_b - (\text{LBF-SEC}^2)/(\text{IN}^2\text{-LBM}^2)$	1875.0	617.0
$R_p - (\text{LBF-SEC}^2)/(\text{IN}^2\text{-LBM}^2)$	389000	17600
$L_p - (\text{LBF-SEC}^2)/(\text{IN}^2\text{-LBM})$	1.83	1.32
Valve Resistance, $R_v = 1/(K_v X^2)$		
$K_v - \text{LBM}^2/(\text{LBF-SEC}^2)$	1.063	3.455
VALVE STROKE, X-IN	0+ .02	0+ 02
PREIGNITER VOLUME - $\text{IN}^3$	$7.17352 \times 10^{-3}$	$5.2666 \times 10^{-3}$
MANIFOLD VOLUME - $\text{IN}^3$	$37.07683 \times 10^{-3}$	$30.4761 \times 10^{-3}$
VAPOR PRESSURE AT 70F - $\text{LBF/IN}^2$	2.2	15
VAPOR DENSITY AT 70F $P_v - \text{LBM/IN}^3$	$10^{-5}$ est	.0326
LIQUID DENSITY AT 70F - $\text{LBM/IN}^3$	.0326	.0522
LIQUID BULK MODULUS, B - $\text{LBF/IN}^2$	$15.308 \times 10^4$	$12.912 \times 10^4$

TABLE C-3 -- continued

COMBUSTOR CONSTANTS, $K - (\text{IN}^2/\text{LBF})^n$	1.26
n - DIMENSIONLESS	0.4
$\left(\frac{U_C C^*}{A_t R T_C}\right) C^* - \text{FT}$	1/0.491
$1/A_t - (\text{LBF-SEC}^2)/(\text{LBM-FT-IN}^2)$	0.053

## APPENDIX D

COMPUTER PROGRAM

A flow diagram showing general features of the computing logic employed is in figure 29 (parts A and B).

A detailed listing of the program follows the logic diagram.

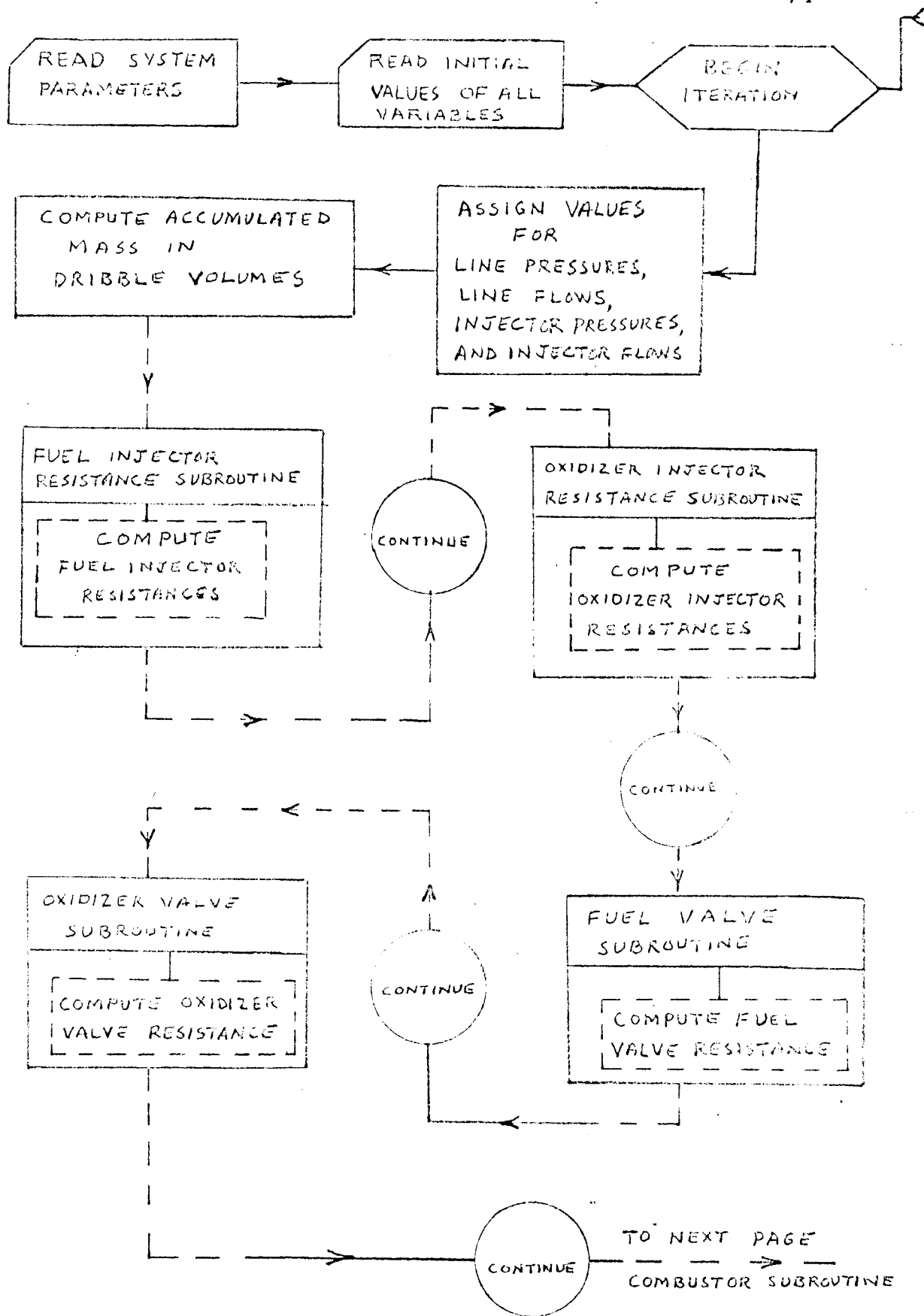


FIGURE 29 - A

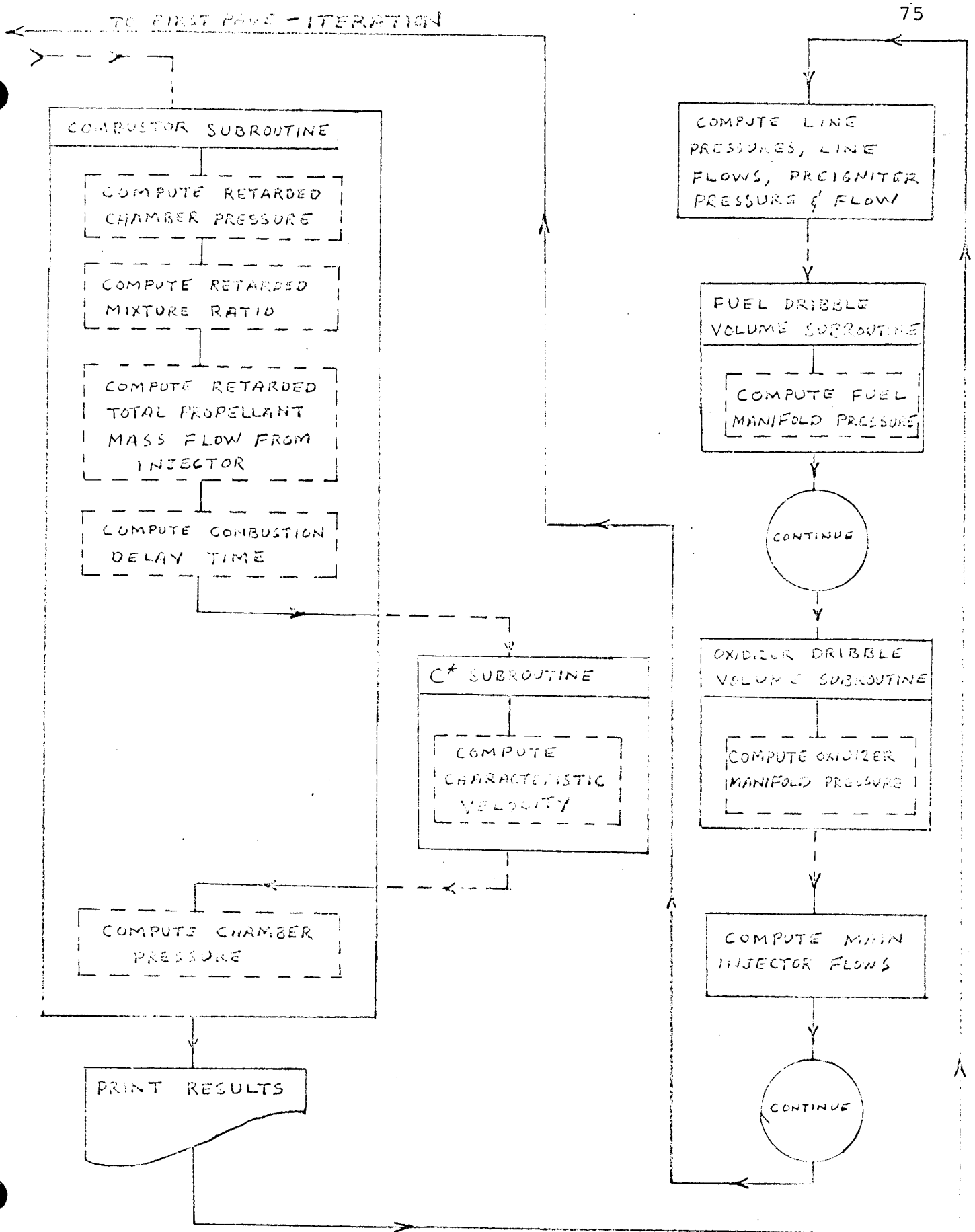


FIGURE 29 - B

## PROGRAM HEAT

```

COMMON      TIME(250) , PCN(250) , XMIX(250) , WL(250) , TAU1
1           ,RW(30) , C (30)
TAU1 = 0.002      $ TAU = TAU1
RW(1) = 0.0      $ C(1) = 0.0
RW(2) = 0.2      $ C(2) = 2925.
RW(3) = 0.4      $ C(3) = 3450.
RW(4) = 0.6      $ C(4) = 3985.
RW(5) = 0.8      $ C(5) = 4450.
RW(6) = 1.0      $ C(6) = 4990.
RW(7) = 1.1      $ C(7) = 5170.
RW(8) = 1.2      $ C(8) = 5300.
RW(9) = 1.4      $ C(9) = 5310.
RW(10) = 1.5      $ C(10) = 5305.
RW(11) = 1.6      $ C(11) = 5260.
RW(12) = 1.7      $ C(12) = 5170.
RW(13) = 1.8      $ C(13) = 5130.
RW(14) = 1.9      $ C(14) = 5070.
RW(15) = 2.0      $ C(15) = 4990.
RW(16) = 2.1      $ C(16) = 4940.
RW(17) = 2.2      $ C(17) = 4900.
RW(18) = 2.3      $ C(18) = 4790.
RW(19) = 2.4      $ C(19) = 4720.
RW(20) = 2.5      $ C(20) = 4640.
RW(21) = 2.6      $ C(21) = 4560.
RW(22) = 2.8      $ C(22) = 4400.
RW(23) = 3.0      $ C(23) = 4230.
RW(24) = 3.2      $ C(24) = 4070.
RW(25) = 3.4      $ C(25) = 3900.
RW(26) = 3.6      $ C(26) = 3710.
RW(27) = 3.8      $ C(27) = 3535.
RW(28) = 4.0      $ C(28) = 3380.
RW(29) = 20.0      $ C(29) = 0.0
795 DO 1000 IJOB = 1 , 100
      READ ( 60 , 800 ) R1 , R3 , R5 , R8 , C2 , C4 ,      C5
800 FORMAT ( 7F10.5 )
      IF ( R1 ) 1001 , 1001 , 801
801 READ(60,802) R01, R03, R05, R08, C02, C04, C05
802 FORMAT ( 7F10.5 )
      C2 = C2 * .000001
      C4 = C4 * .000001
      C5 = C5 * .000001
      C02 = C02 * .000001
      C04 = C04 * .000001
      C05 = C05 * .000001
      READ ( 60,803 ) AL1, AL2, AL4, AL6, AL9, PT
803 FORMAT ( 6F10.5 )
      READ ( 60,804 ) AL01, AL02, AL04, AL06, AL09, POT
804 FORMAT ( 6F10.5 )
      READ ( 60,805 ) BRK1,BRK2,BRK3,BRK4,BK01,BK02,BK03,BK04
805 FORMAT ( 8F10.5 )
      READ ( 60,806 ) CLOSEP , UP , MILSEC
806 FORMAT ( 2F10.5 , I3 )
      IFIN = MILSEC * 100 + 1
      AM = 0.0
      XMO = 0.0
      K=0
      PCNN = 0.0
      DT = .000001
      IP = 9

```



```

PIN = P1    $ P2N = P1    $ P3N = P1    $ P4N = P1    $ P5N = P1
P6N = P1    $ P7N = P1    $ P8N = 0.0    $ P9N = 0.0    $ P10N = 0.0
W1N = 0.0    $ W3N = 0.0    $ W5N = 0.0    $ W7N = 0.0    $ W8 = 0.0
W9N = 0.0    $ W11N = 0.0    $ W1(1) = 0.0    $ PCH(1) = 0.0    $ P01N = P01
P02N = P01    $ P03N = P01    $ P05N = P01    $ P06N = P01    $ P07N = P01
P08N = 0.0    $ P09N = 0.0    $ P010N = 0.0    $ W01N = 0.0    $ W03N = 0.0
W05N = 0.0    $ W07N = 0.0    $ W08 = 0.0    $ W09N = 0.0    $ W011N = 0.0
P04N = P01

```

```

DO 999 IOK = 1,IFIN
2 K = K + 1
IP = IP + 1
P1 = P1N    $ P2 = P2N    $ P3 = P3N    $ P5 = P5N    $ P6 = P6N
P4 = P4N    $ P04 = P04N
P7 = P7N    $ P8 = P8N    $ P9 = P9N    $ P10 = P10N    $ P01 = P01N
P02 = P02N    $ P03 = P03N    $ P05 = P05N    $ P06 = P06N    $ P07 = P07N
P08 = P08N    $ P09 = P09N    $ P010 = P010N    $ W1 = W1N    $ W3 = W3N
W5 = W5N    $ W7 = W7N    $ W8 = W7N - W9N    $ W9 = W9N    $ W11 = W11N
W01 = W01N    $ W03 = W03N    $ W05 = W05N    $ W07 = W07N
W08 = W07N - W09N    $ W09 = W09N    $ W011 = W011N    $ W12 = W9 + W11
W012 = W09 + W011
AM = AM + DT * ( W8 - W11 )
XMO = XMO + DT * ( W08 - W011 )
CALL RSHIF ( XM , R10 , R11 , L10 , XF , UP )
CALL RSHIF0 ( XMO , R010 , R011 , L100 , X0 , UP )
L2 = K - 1
T123 = L2
T = DT * T123
CALL VALVES ( 1 , XF , X0 , R7 , R07 , BRK1,BRK2,BRK3,BRK4,
1 BR01, BR02, BR03, BR04, CL0SE )
CALL RETARD ( TAU , XMIAN , XERE , K , PCAN , DT , W12 , W012 ,
1 L10 , L100 )
IF( IP - 20 ) G2 , G1 , G1
81 IP = 0
WRITE ( 61 , 77 ) P1 , P01 , W1 , W01
77 FORMAT ( 1X , 6H P1 = , E20.9 , 6H P01 = , E20.9 , 6H W1 = ,
1 E20.9 , 6H W01 = , E20.9 )
WRITE ( 61 , 5 ) P2 , P02
5 FORMAT ( 1X , 6H P2 = , E20.9 , 6H P02 = , E20.9 )
WRITE ( 61 , 78 ) P3 , P03 , W3 , W03
78 FORMAT ( 1X , 6H P3 = , E20.9 , 6H P03 = , E20.9 , 6H W3 = ,
1 E20.9 , 6H W03 = , E20.9 )
WRITE ( 61 , 6 ) P4 , P04
6 FORMAT ( 1X , 6H P4 = , E20.9 , 6H P04 = , E20.9 )
WRITE ( 61 , 7 ) P5 , P05 , W5 , W05
7 FORMAT ( 1X , 6H P5 = , E20.9 , 6H P05 = , E20.9 , 6H W5 = ,
1 E20.9 , 6H W05 = , E20.9 )
WRITE ( 61 , 79 ) P6 , P06
79 FORMAT ( 1X , 6H P6 = , E20.9 , 6H P06 = , E20.9 )
WRITE ( 61 , 80 ) P7 , P07 , W7 , W07
80 FORMAT ( 1X , 6H P7 = , E20.9 , 6H P07 = , E20.9 , 6H W7 = ,
1 E20.9 , 6H W07 = , E20.9 )
WRITE ( 61 , 8 ) P8,P08 , W8 , W08
8 FORMAT ( 1X , 6H P8 = , E20.9 , 6H P08 = , E20.9 , 6H W8 = ,
1 E20.9 , 6H W08 = , E20.9 )
WRITE ( 61 , 9 ) P9 , P09 , W9 , W09
9 FORMAT ( 1X , 6H P9 = , E20.9 , 6H P09 = , E20.9 , 6H W9 = ,
1 E20.9 , 6H W09 = , E20.9 )
WRITE ( 61 , 10 ) P10 , P010 , W11 , W011
10 FORMAT ( 1X , 6H P10 = , E20.9 , 6H P010 = , E20.9 , 6H W11 = ,
1 E20.9 , 6H W011 = , E20.9 )

```

```

WRITE ( 01 , 40 )  AF , X0 , P7 , R07
40 FORMAT ( 1X , 6H AF = , E20.9 , 6H X0 = , E20.9 , 6H R7 = ,
1 E20.9 , 6H R07 = , E20.9 )
WRITE ( 01 , 41 )  IAU , APIXN , WLRN , PCHN , I
41 FORMAT ( 1X , 6H IAU = , E20.9 , 6H APIXN = , E20.9 , 6H WLRN = ,
1 E20.9 , 6H PCHN = , E20.9 , 6H I = , F9.7 )
WRITE ( 01 , 705 )  XM , XMO
705 FORMAT ( 1X , 6H XM = , E20.9 , 6H XMO = , E20.9 , // )
C TURN SENSE SWITCH ON , WAIT FOR COMPUT TO STOP TURN OFF ABOUTS ONLY PROBLEM IN
C PROGRESS
GO TO ( 82 , 797 ) SSWITCH(1)
797 PAUSE
GO TO 795
82 P2N = P2 + D1 * ( A1 - A3 ) / C2
P02N = P02 + D1 * ( A01 - A03 ) / C02
A1N = A1 + D1 * ( P1 - P2 ) / A01
W01N = W01 + D1 * ( P01 - P02 ) / A01
P1N = P1 - W1N * ABSF( W1N ) * R1
P01N = P01 - W01N * ABSF( W01N ) * R01
P4N = P4 + D1 * ( A3 - A5 ) / C4
P04N = P04 + D1 * ( A03 - A05 ) / C04
W3N = W3 + D1 * ( P2 - P3 ) / A02
W03N = W03 + D1 * ( P02 - P03 ) / A02
P3N = P3N + R3 * W3N * ABSF( W3N )
P03N = P04N + W03 * W03N * ABSF( W03N )
P5N = P5 + D1 * ( A5 - A7 ) / C5
P05N = P05 + D1 * ( A05 - A07 ) / C05
W5N = W5 + D1 * ( P4N - P5N ) / A04
W05N = W05 + D1 * ( P04N - P05N ) / A04
IF ( AF - A01 ) 90 , 90 , 92
92 TERM1 = A00 / D1
TERM2 = TERM1 / A7
TERMS = ( P3 - P5 - TERM1 * A7 ) / A7
W7N = ( - TERM2 + SQRT( TERM2**2 - 4. * TERMS ) ) / 2.
P5N = P5N - A5 * ABSF( W7N ) * W7N
P7N = P5N - A05 * ( W7N - A7 ) / D1
GO TO 94
90 W7N = 0.0
P5N = P5N - A5 * ABSF( W7N ) * W7N
P7N = P5N - A05 * ( W7N - A7 ) / D1
94 IF ( X0 - 0.0001 ) 96 , 96 , 96
96 TERM10 = A006 / D1
TERM20 = TERM10 / A07
TERM30 = ( P05 - P06 - TERM10 * A07 ) / A07
W07N = ( - TERM20 + SQRT( TERM20**2 - 4. * TERM30 ) ) / 2.
P05N = P05N - R05 * ABSF( W07N ) * W07N
P07N = P05N - A006 * ( W07N - A07 ) / D1
GO TO 99
90 W07N = 0.0
P05N = P05N - R05 * ABSF( W07N ) * W07N
P07N = P05N - A006 * ( W07N - A07 ) / D1
99 P9N = P8 - R8 * ABSF( W9 ) * W9
IF( P9N ) 107 , 107 , 109
107 P9N = 0.0
109 W9N = W9 + D1 * ( P9 - PCHN ) / A09
IF ( ABSF(W09) - .0000000001 ) 210 , 212 , 212
210 P09N = P08
GO TO 214
212 P09N = P08 - R08 * ABSF( W09 ) * W09
214 IF( P09N ) 122 , 122 , 124
122 P09N = 0.0
124 W09N = W09 + D1 * ( P09 - PCHN ) / A09

```

```

      CALL PR ( XM , P10N , P8 , PCHN , R11 , XF , DI )
      CALL PRO ( X80 , P010N , P08 , PCHN , W011 , X0 , DI )
      P8N = P10N + R10 * ( X7N- X9N ) * ABSF( W7N- W9N )
      P08N = P010N + R010 * ( W07N- W09N ) * ABSF( W07N- W09N )
      CONS = ABSF ( P10N- PCHN )
      CONSO = ABSF ( P010N- PCHN )
      IF ( CONS - .001 ) 100 , 100 , 110
110  W11N = SQRTF ( CONS / R11 ) * ( P10N- PCHN ) / CONS
      GO TO 120
100  W11N = 0.0
120  IF ( CONSO - .001 ) 130 , 130 , 140
130  W011N = 0.0
      GO TO 999
140  W011N = SQRTF ( CONSO / R011 ) * ( P010N- PCHN ) / CONSO
      IF ( W11N ) 310 , 312 , 312
310  W11N = 0.0
312  IF ( W011N ) 314 , 999 , 999
314  W011N = 0.0
999  CONTINUE
1000 CONTINUE
1001 WRITE ( 61 , 1002 )
1002 FORMAT ( 10X , 4H END )
      END

```

FORTRAN DIAGNOSTIC RESULTS FOR HEAT

L STATEMENT NUMBERS

4

2

```

SUBROUTINE RETARD ( TAU , AMIXN , WLR , N , PCHN , D1 , W12 ,
1  W012 , LIM , LIQU )
COMMON TIME(250) , PCH(250) , AMIX(250) , WL(250) , TAU1
1  WLR(30) , C(30)
IF ( N - 250 ) 5 , 5 , 10
5  IN = N
GO TO 20
10 M = N / 250
IN = N - M * 250
20 J1 = N - 1
J2 = J1
TIME = J2 * D1
TIMEK = TIME - TAU
TIME(IN) = TIME
IF ( W12 ) 1 , 1 , 2
2 IF ( W012 ) 1 , 4 , 4
4 AMIX(IN) = W012 / W12
WL(IN) = W012 * W12
GO TO 3
1 AMIX(IN) = 0.0
WL(IN) = 0.0
3 IF ( TIMEK .LT. 23 , 23
23 DO 40 I = 1 , 250
IF ( IN - I , 25 , 25 , 50
50 M = IN - I
GO TO 51
25 M = IN - 1 * 250
61 IF ( TIME(M) - TIMEK ) 33 , 33 , 40
33 IF ( M - 1 ) 35 , 35 , 37
35 M2 = 250
GO TO 42
37 M2 = M - 1
GO TO 42
40 CONTINUE
WRITE ( 61 , 41 )
41 FORMAT ( 'ION RETARD TIME WRONG )
C
42 F = ( TIMEK - TIME(M2) ) / ( TIME(M) - TIME(M2) )
AMIXK = AMIX(M2) + F * ( AMIX(M) - AMIX(M2) )
PCHK = PCH(M2) + F * ( PCH(M) - PCH(M2) )
WLR = WL(M2) + F * ( WL(M) - WL(M2) )
GO TO 43
44 AMIXK = 0.0
PCHK = 0.0
WLR = 0.0
C
C 45 TAU = 1002 / ( 1. + 1.26 * PCHN**.4 )
C
45 TAU = 150 * ( 1. - ( 1. + 1.26 * PCHN **.4 ) / ( 1. + 1.26 * PCHK
1 **.4 ) ) * D1
CALL CSRE ( AMIXK , CSRE )
IF ( CSRE ) 55 , 55 , 52
52 PCHN = PCHN + ( CSRE * D1 / 2.04 ) * ( ( 1. + 1.26 * PCHN **.4
1 ) * WLR / ( 1. + 1.26 * PCHK **.4 ) * .053 * CSRE ) - PCHN )
PCH(1N) = PCHN
GO TO 53
53 PCH(1N) = 0.0
PCHN = 0.0
60 AMIXN = AMIX(1N)
RETURN
END

```

```

      SUBROUTINE CSTAR ( AMIARE , CSRE )
      COMMON /TIME(250) , PCH(250) , APLX(250) , WL(250) , FAU1
      I = 1
      IF ( AMIARE - 20. ) 40 , 40 , 15
      15 CSRE = 0.0
      GO TO 50
      40 DO 20 I = 1 , 50
      I = 1
      IF ( AMIARE - RW(1) ) 30 , 20 , 20
      20 CONTINUE
      30 F = ( AMIARE - RW(N-1) ) / ( RW(N) - RW(N-1) )
      CSRE = C (N-1) + F * ( C (N) - C (N-1) )
      50 RETURN
      END

```

FORTRAN DIAGNOSTIC RESULTS FOR CSTAR

MSUS

```

SUBROUTINE PR ( XM , P10 , P8 , PCHN , W11 , XF , DT )
  SL1 = .00169 / 10000.
  DEL = .00121
  SL2 = .0000079 / 10000.
  PVF = 2.2
  BK1 = PVF * SL1
  BK2 = BK1 + DEL
  IF( AM - BK1 ) 10 , 10 , 15
10 P10 = XM / SL1
  XMV= 0.0
  GO TO 30
15 IF( AM - BK2 ) 20 , 20 , 25
20 IF ( XF - .000000001 ) 50 , 50 , 45
50 P10 = PVF
  GO TO 30
45 P10 = PVF
80 GO TO 30
25 W = SQRT( ABSF( ( P8-PCHN ) / 3525. ) )
  P10 = P8 - ( 1650. * W**2 ) * ( P8-PCHN ) / ABSF(P8-PCHN)
  XMV= 0.0
  IF(P10 - PVF ) 40 , 40 , 30
40 AM = .0000000001
30 RETURN
END

```

FORTRAN DIAGNOSTIC RESULTS FOR PR

L STATEMENT NUMBERS

80

```
SUBROUTINE PRO ( XMO , PO10 , PO8 , PCHN , WO11 , XO , DT )
  SL1 = .00147 / 10000.
  DEL = .001569
  SL2 = .000120 / 10000.
  PVF = 15.
  BK1 = PVF * SL1
  BK2 = BK1 + DEL
  IF( XMO - BK1 ) 10 , 10 , 15
10 PO10 = XMO / SL1
  XMOV= 0.0
  GO TO 30
15 IF( XMO - BK2 ) 20 , 20 , 25
20 IF ( XO - .000000001 ) 50 , 50 , 45
50 PO10 = PVF
  GO TO 30
45 PO10 = PVF
80 GO TO 30
25 W = SQRT( ABSF( ( PO8 - PCHN ) / 901. ) )
  PO10 = PO8 - ( 284. * W **2 ) * ( PO8-PCHN ) / ABSF(PO8-PCHN)
  XMOV= 0.0
  IF(PO10 - PVF ) 40 , 40 , 30
40 XMO = BK2 - .000000001
30 RETURN
END
```

## FORTRAN DIAGNOSTIC RESULTS FOR PRO

## STATEMENT NUMBERS

80

```
SUBROUTINE RSHIF ( XM , R10 , R11 , LIQ , XF , UP )  
DEL = .00121  
BK1 = 2.2 * .00169 / 10000.  
BK2 = BK1 + DEL  
IF ( XM - BK1 ) 10 , 10 , 15  
10 R10 = 165000.  
R11 = 187500.  
LIQ = 1  
GO TO 30  
15 IF ( XM - BK2 ) 20 , 20 , 25  
20 R10 = 1650.  
R11 = 187062. - 1530000000. * XM  
IF ( XF - .000000001 ) 50 , 50 , 30  
50 IF(UP) 60 , 60 , 70  
C   DOWN FIRING ENGINE  
60 R11 = 1875.  
LIQ = 1  
GO TO 30  
C   UP FIRING ENGINE  
70 R11 = 187500.  
LIQ = 1  
GO TO 30  
25 R10 = 1650.  
R11 = 1875.  
LIQ = -1  
30 RETURN  
END
```

FORTTRAN DIAGNOSTIC RESULTS FOR RSHIF

RRUKS



```
SUBROUTINE RSHIFO( XMO , RO10 , RO11 , LIQ0 , XO , UP )  
DEL = .001569  
BK1 = 15. * .01470 / 10000.  
BK2 = BK1 + DEL  
IF ( XMO - BK1 ) 10 , 10 , 15  
10 RO10 = 28400.  
RO11 = 61700.  
LIQ0 = 1  
GO TO 30  
15 IF ( XMO - BK2 ) 20 , 20 , 25  
20 RO10 = 284.  
RO11 = 62468. - 38900000. * XMO  
IF ( XO - .000000001 ) 50 , 50 , 30  
50 IF(UP) 60 , 60 , 70  
C DOWN FIRING ENGINE  
60 RO11 = 617.  
LIQ = 1  
GO TO 30  
C UP FIRING ENGINE  
70 RO11 = 61700.  
LIQ = 1  
GO TO 30  
25 RO10 = 284.  
RO11 = 617.  
LIQ0 = -1  
30 RETURN  
END
```

FORTRAN DIAGNOSTIC RESULTS FOR RSHIFO

RRORS

```
SUBROUTINE RES ( PA , PB , R , W )  
X = ( PA - PB ) * R  
Z = ABSF ( PA - PB ) - .0000000001  
IF ( Z ) 2 , 2 , 1  
1 Y = ABSF ( X )  
W = SQRTF ( Y ) * X / Y  
GO TO 3  
2 W = 0.0  
3 RETURN  
END
```

FORTRAN DIAGNOSTIC RESULTS FOR RES

RRORS

```

SUBROUTINE VALVES ( T , XF , X0 , R7 , R07 , BKF1,BKF2,BKF3,
1 BKF4, BK01, BK02, BK03, BK04, CLOSEF )
  SL = .02 / .0015
  FRAC = T / ( BKF4 + CLOSEF )
  R = FRAC
  Z = R
  Z1 = FRAC - Z
  T = Z1 * ( BKF4 + CLOSEF )
  IF ( T - BKF1 ) 30 , 30 , 32
30 XF = 0.0
  GO TO 50
32 IF ( T - BKF2 ) 34 , 34 , 36
34 XF = ( T - BKF1 ) * SL
  GO TO 50
36 IF ( T - BKF3 ) 38 , 38 , 40
38 XF = 0.02
  GO TO 50
40 IF ( T - BKF4 ) 42 , 42 , 44
42 XF = .02 - ( T - BKF3 ) * SL
  GO TO 50
44 XF = 0.0
50 IF ( XF ) 55 , 52 , 55
52 R7 = 1000000000. / .0000001
  GO TO 60
55 R7 = 1. / ( 1.063 * XF **2 )
60 IF ( T - BK01 ) 62 , 62 , 64
62 X0 = 0.0
  GO TO 80
64 IF ( T - BK02 ) 66 , 66 , 68
66 X0 = ( T - BK01 ) * SL
  GO TO 80
68 IF ( T - BK03 ) 70 , 70 , 72
70 X0 = .02
  GO TO 80
72 IF ( T - BK04 ) 74 , 74 , 76
74 X0 = .02 - ( T - BK03 ) * SL
  GO TO 80
76 X0 = 0.0
80 IF ( X0 ) 90 , 88 , 90
88 R07 = 1000000000. / .0000001
  GO TO 100
90 R07 = 1. / ( 3.455 * X0 ** 2 )
100 RETURN
  END

```

FORTRAN DIAGNOSTIC RESULTS FOR VALVES

ERRORS  
 0.00  
 0

## NOMENCLATURE

Symbols

$a$	-	Acoustic Velocity in Fluid
$A$	-	Cross-sectional Area
$B$	-	Bulk Modulus
$C$	-	Fluid Capacitance
$C^*$	-	Characteristic Velocity
$D$	-	Diameter
$E$	-	Young's Modulus of Elasticity
$f$	-	Friction Factor
$F$	-	Force
$G$	-	Mass Velocity
$K$	-	Combustion Rate Constant
$l$	-	Length Measured in Flow Direction
$L$	-	Fluid Flow Inductance
$P$	-	Pressure
$q$	-	Chemical Reaction Rate
$R$	-	Fluid Flow Resistance
$R$	-	(In Combustor Equation) Specific Gas Constant
$R_w$	-	Oxidizer/fuel Ratio
$S$	-	Surface Area
$t$	-	Time
$T$	-	Temperature
$U$	-	Unit Step Function
$V$	-	Fluid Velocity
$V$	-	Volume of Fluid Region
$\dot{W}$	-	Fluid Mass Flow Rate

$W$  - Mass Content  
 $W_L$  - Liquid Mass  
 $W_V$  - Vapor Mass  
 $x$  - Valve Stroke or Position in Feed Line  
 $\alpha$  - Stream Tube Divergence Angle  
 $\delta$  - Dirac Delta Function  
 $\Delta$  - Difference  
 $\tau$  - Combustion Delay Time  
 $\tau_s$  - Shear Stress at Wall

Subscripts

$a$  - Entrance  
 $b$  - Exit  
 $c$  - Combustion Chamber  
 $e$  - Equivalent  
 $F$  - Fuel  
 $i$  - Inside  
 $k$  - Summation Index  
 $L$  - Liquid  
 $l$  - Line  
 $m$  - Manifold  
 $n$  - Number, (For Combustion) Interaction Parameter  
 $o$  - Outside  
 $ox$  - Oxidizer  
 $p$  - Preigniter  
 $t$  - Nozzle Throat  
 $v$  - Vapor

- 1 - Upstream
- 2 - Downstream

NOTE:

A Bar ( $\bar{\phantom{x}}$ ) denotes the instantaneous value of a spatially averaged quantity.

An Arrow ( $\vec{\phantom{x}}$ ) denotes a vector quantity.

A ( $\propto$ ) denotes a proportionality.

## REFERENCES

1. Perlee, Henry E. and Theodore Christos: Summary of Literature Survey of Hypergolic Ignition Spike Phenomena, Phase 1 - Final Report, U.S. Dept. of the Interior, Bureau of Mines, Pittsburg, Penn., April 8 to Dec. 31, 1965.
2. Bowling, R. C. and R. K. Rose: Dynamic Interaction Analysis and Computer Model LM Reaction Control Propulsion System, Advanced Technology Laboratories, General Electric Company, March, 1965.
3. Streeter, V. L. and E. B. Wylie: Hydraulic Transients, McGraw-Hill Book Company, Inc., 1967.
4. Streeter, V. L. (Editor-in-chief): Handbook of Fluid Dynamics, McGraw-Hill Book Company, Inc., 1961.
5. Blackburn, John F.; Reethof, Gerhard; and Shearer, J. Lowen: Fluid Power Control, Technology Press of M.I.T. and John Wiley and Sons, Inc., New York, 1960.
6. Crocco, L. and Sin-I Cheng: Theory of Combustion Instability In Liquid Propellant Rocket Motors, Butterworths Scientific Publications, 1956.
7. Sherrill, H. L.: Final Report For LM-RCS Engine Injector Simulation on a Hybrid Computer.